Computational and Structural Biotechnology Journal 23 (2024) 2388–2406

Contents lists available at ScienceDirect

Computational and Structural Biotechnology Journal

journal homepage: www.elsevier.com/locate/csbj

A novel cathelicidin TS-CATH derived from *Thamnophis sirtalis* combats drug-resistant gram-negative bacteria *in vitro* and *in vivo*

Jian Wang, Meina Zhang, Chao Li, Mengyuan Liu, Yixin Qi, Xiaolin Xie, Changlin Zhou *, Lingman Ma *

Institution of all authors: College of Life Science and Technology, China Pharmaceutical University, Nanjing, Jiangsu 211198, China

ARTICLE INFO

Keywords:
Cathelicidin antimicrobial peptides
Drug-resistant bacteria
Bacteremia
Wound infection
Respiratory chain
ROS

ABSTRACT

Antimicrobial peptides are promising therapeutic agents for treating drug-resistant bacterial disease due to their broad-spectrum antimicrobial activity and decreased susceptibility to evolutionary resistance. In this study, three novel cathelicidin antimicrobial peptides were identified from *Thamnophis sirtalis*, *Balaenoptera musculus*, and *Lipotes vexillifer* by protein database mining and sequence alignment and were subsequently named TS-CATH, BM-CATH, and LV-CATH, respectively. All three peptides exhibited satisfactory antibacterial activity and broad antibacterial spectra against clinically isolated *E. coli*, *P. aeruginosa*, *K. pneumoniae*, and *A. baumannii in vitro*. Among them, TS-CATH displayed the best antimicrobial/bactericidal activity, with a rapid elimination efficiency against the tested drug-resistant gram-negative bacteria within 20 min, and exhibited the lowest cytotoxicity toward mammalian cells. Furthermore, TS-CATH effectively enhanced the survival rate of mice with ceftazidime-resistant *E. coli* bacteremia and promoted wound healing in meropenem-resistant *P. aeruginosa* infection. These results were achieved through the eradication of bacterial growth in target organs and wounds, further inhibiting the systemic dissemination of bacteria and the inflammatory response. TS-CATH exhibited direct antimicrobial activity by damaging the inner and outer membranes, resulting in leakage of the bacterial contents at super-MICs. Moreover, TS-CATH disrupted the bacterial respiratory chain, which inhibited ATP synthesis and induced ROS formation, significantly contributing to its antibacterial efficacy at sub-MICs. Overall, TS-CATH has potential for use as an antibacterial agent.

1. Introduction

The golden age of antibiotic discovery has elapsed, and we are heading for an "era of antibiotic resistance" [1]. Since penicillin was discovered in 1929, the application of various small-molecule antibacterial drugs and the iterative upgrading of synthetic and semisynthetic antibiotics have significantly improved the treatment rates of bacterial infections in humans and animals in the following 75 years. However, in the 21st century, the irrational use of antibiotics for the treatment of infection and the abuse of antibiotics in the animal husbandry industry and their associated adverse effects also followed. Today, a variety of antibiotic-resistant bacteria are found worldwide, and antimicrobial resistance (AMR) has become a global health emergency [2].

Bacteria acquire antibiotic resistance through mutations, horizontal gene transfer, and plasmid transmission via membrane vesicles [3–5]. This leads to cross-resistance, making the bacteria resistant to multiple antibiotics. Multidrug-resistant organisms (MDRO), which are resistant to three or more antibiotics, are common in the antibiotic resistance era [6]. After 2–3 years of clinical antibiotic use, drug-resistant strains emerged, including MRSA strains resistant to linezolid and daptomycin [7–9]. The excessive use of colistin in agriculture threatens polymyxins, the last resort against multidrug-resistant gram-negative bacteria [10]. This can promote the spread of drug resistance genes such as mcr-1 [11, 12]. The development of new antibiotics lags behind the spread of bacterial resistance, necessitating the discovery of novel antibacterial drugs [6].

Antimicrobial peptides (AMPs) are short (12–100 amino acids) and positively charged (+2 to +9) amphiphilic molecules found in single-celled microorganisms, insects, invertebrates, plants, amphibians, birds, fish, and mammals, including humans, as part of their first line of defense [13]. Also known as host defense peptides (HDPs), they exhibit an extraordinarily broad range of antimicrobial activities against both

* Corresponding authors.
E-mail addresses: cl_zhou@cpu.edu.cn (C. Zhou), 1620174416@cpu.edu.cn (L. Ma).

https://doi.org/10.1016/j.csbj.2024.05.020
Received 28 December 2023; Received in revised form 8 May 2024; Accepted 13 May 2024
Available online 17 May 2024

gram-positive and gram-negative bacteria as well as fungi, viruses, and unicellular protozoa [14,15]. AMPs selectively interact with bacterial membranes via electrostatic interactions and then efficiently kill microbial pathogens by forming pores at the membrane surface to cause loss of membrane integrity, which also contributes to the translocation of AMPs into the cytoplasm, where they target key intracellular processes, including DNA/RNA and protein synthesis, protein folding, enzymatic activity, and/or cell wall synthesis [16,17]. In addition to direct antimicrobial activity, several AMPs can modulate the innate immune responses of the host and thereby indirectly promote pathogen clearance [18]. AMPs are much more refractory to resistance than are conventional antibiotics due to their biochemical properties, pharmacodynamics, and multimechanism characteristics [19–21]. Thus, AMPs offer promising alternatives to standard therapies, such as anti-infectives and immunomodulatory agents [16,20,22].

Cathelicidins are among the most important host defense peptide families and play important roles in the innate immune response [23]. The majority of cathelicidins are linear with an α-helical structure (23–37 amino acids) and are amphipathic, cationic peptides with a hydrophobic surface that contributes to interactions with and perturbs the membranes of anionic surfaces [16]. Cathelicidins maintain broad-spectrum antimicrobial activity and are equipped with other biological activities, such as inducing chemotaxis of various immune cells [24,25], inducing apoptosis of infected cells [26], and promoting wound healing [27] and the re-epithelialization of wounds [28]. Multifunctional cathelicidins have shown promising potential for the development of new therapeutic agents. Several cathelicidins and their derivatives, such as human cathelicidin LL-37, have been extensively studied and evaluated in clinical trials. Its therapeutic properties have been investigated, highlighting its potential in various medical applications. [16].

Cathelicidins have been identified in many vertebrates, including cows, pigs, rabbits, sheep, humans, mice, monkeys, and horses [29–31]. Cathelicidin-related protein precursors are characterized by a signal sequence in the N-terminus with a highly conserved cathelin domain, while substantial heterogeneity in the C-terminal domain encodes the activity of the mature peptide [32]. Owing to the highly conserved cathelin domain, it is possible to find new cathelicidins by sequence alignment against protein databases from other species [33–35]. Unlike poisonous snakes, which are the main source of many cathelicidin peptides [35], nonvenomous snakes are more easily obtainable, and peptides derived from them are rarely reported. In addition, as a rich source of novel and bioactive metabolites, marine organisms have attracted a great deal of attention; however, cathelicidin peptides from marine mammals are also seldom reported. Here, we screened three novel cathelicidin antimicrobial peptides and obtained TS-CATH, a peptide with effective antibacterial activity and negligible cytotoxicity *in vitro*. TS-CATH not only triggered the permeability of the inner and outer membranes of bacteria and destroyed the integrity of the membranes but also disturbed the bacterial respiratory chain, inhibited ATP production, and induced ROS formation, which enhanced antibacterial activity.

2. Materials and methods

2.1. Identification and characterization of novel cathelicidins

A cathelicidin-related protein precursor derived from *Ophiophagus hannah* (*O. hannah*, GenBank: ACF21002.1) was used to find a novel cathelicidin-related protein precursor derived from other species via the BLAST tool at the National Center for Biotechnology Information (NCBI) website as described previously [33,35,36]. Briefly, the cathelicidin sequence of *O. hannah* (GenBank: ACF21002.1) was used as a template to search for cathelicidin-like sequences via BLAST against the nonredundant protein sequence database of *Thamnophis sirtalis* (txid: 35019), *Balaenoptera musculus* (txid: 9771), and *Lipotes vexillifer* (txid: 118797). Then, the complete structures of the cathelicidin-like sequences XP_013912467.1, XP_036725121.1, and XP_007446280.1 were selected because of rich in the hydrophobicity, hydrophobic moment and net charge, which are crucial properties of α-helical AMPs (Table S1). Subsequently, the corresponding cathelicidin-like sequences and other representative cathelicidins were imported into MEGA 7 software for multisequence alignment. The ClustalW tool was used for alignment, and four conserved cysteine residues in the cathelin domain were verified [33].

2.2. Structure characterization and modeling

Elastase-sensitive residues were predicted using Peptide Cutter (https://web.expasy.org/peptide_cutter/). This tool operates based on the rules established by Keil [37] and subsequently validated by Barrett et al. [38]. The mature peptide regions of cathelicidin sequences located at the C-terminus were truncated by the predicted elastase-sensitive residues and named TS-CATH, BM-CATH, and LV-CATH, respectively [33]. Three-dimensional (3D) structures were generated by SWISS-MODEL (https://swissmodel.expasy.org/). The physicochemical properties and helical wheel projections of the peptides were estimated by helical wheel diagrams (https://heliquest.ipmc.cnrs.fr/cgi-bin/ComputParams.py).

2.3. Peptides

The peptides TS-CATH, BM-CATH, and LV-CATH were synthesized by standard Fmoc solid-phase synthesis protocols (GL Biochem Co., Ltd., Shanghai, China) to a purity of $> 98\%$.

2.4. Bacterial strains, cells and mice

Escherichia coli (*E. coli*) ATCC 25922, *Pseudomonas aeruginosa* (*P. aeruginosa*) ATCC 27853, *Klebsiella pneumoniae* (*K. pneumoniae*) ATCC 13883, and *Staphylococcus aureus* (*S. aureus*) ATCC 29213 were obtained from the American Type Culture Collection (ATCC). All test clinical strains were isolated from clinical specimens and identified by Jiangsu Women and Children Health Hospital (JWCHH) (Nanjing, China) or Fuyang People's Hospital (Anhui, China). The bacterial strains used in this study are listed in Table S3.

Human umbilical vein endothelial cells (HUVECs), human normal lung epithelial cells (BEAS-2B), mouse subcutaneous connective tissue cells (L929), and human hepatic cells (L02) were purchased from ATCC. The cells were cultured in DMEM (Gibco, Carlsbad, CA, USA) supplemented with 10% FBS and 1% penicillin/streptomycin. Sheep red blood cells (sRBCs) were purchased from SenBeiJia Biological Technology Co., Ltd. (Nanjing, China).

ICR mice (aged 5–6 weeks, half male and half female) were purchased from the Laboratory Animal Center of Yangzhou University (Yangzhou, China) and housed in a rodent facility at 22 ± 1 °C with a 12 h light—dark cycle. All animal experiments were carried out in accordance with the experimental animal administrative committee of China Pharmaceutical University.

2.5. CD assay

The secondary structures of the peptides were evaluated by circular dichroism (CD) spectroscopy (J-820; Jasco, Tokyo, Japan). Peptides were dissolved in deionized water or 25 mM SDS at a final concentration of 0.1 mg/ml. A quartz dish with a diameter of 0.1 cm and a slit of 1 nm was used, and the CD spectra were scanned from 190 to 260 nm at a scanning speed of 100 nm/min.

2.6. Agar dilution assay

An agar dilution assay issued by the Clinical & Laboratory Standards

Institute (CLSI) [39] was performed to determine the minimum inhibitory concentrations (MICs) for clinical isolate strains. Briefly, all strains were cultured overnight at 37 °C to the logarithmic phase, and the bacteria were diluted to 2×10^7 CFU/ml before use. Moreover, 2-fold serial dilutions of peptides were mixed with melted MHA (Mueller–Hinton agar) at final concentrations ranging from 128 to 0.5 μg/ml. A 96-well plate inoculated with bacterial suspensions was placed on the platform of a multipoint inoculator (SAKUMA, Japan), and the various bacterial suspensions were dotted on the surface of the agar plate (approximately 10^4 CFU per spot). The plate was then incubated at 37 °C for 20 h, and the MICs were recorded as the lowest concentrations at which bacterial growth was completely inhibited. This experiment was repeated twice.

2.7. Broth microdilution assay

The MICs of the peptides and antibiotics were determined by a broth microdilution assay issued by the CLSI [39]. Briefly, the bacteria were cultured overnight in MHB (Mueller–Hinton broth) at 37 °C to the logarithmic growth phase, and the bacteria were diluted to 2×10^5 CFU/ml. Similarly, 2-fold serial dilutions of peptides and antibiotics (100 μl) were inoculated in a 96-well plate and mixed with an equal volume of bacterial suspension (approximately 10^4 CFU in each well). After 20 h of coincubation at 37 °C, the MIC was determined by measuring the absorbance at OD_{600}. Specifically, *H. pylori* SS1 was cultured in brain-heart infusion (BHI) broth supplemented with 7% heat-inactivated FBS at 37 °C with AnaeroPack-MicroAero for 48 h [40]; *S. pneumoniae* was cultured in Todd–Hewitt Yeast (THY) broth in a 37 °C (5% CO_2) incubator for 20 h.

The minimum bactericidal concentration (MBC) was determined after the MIC was confirmed. That is, a 200 μl mixture in which microbial growth was not detected was mixed with melted Mueller–Hinton agar in a sterile plate, and the plate was incubated at 37 °C for 20 h. The MBC value was recorded when there were fewer than 5 bacterial colonies on the plate. All the tests were performed in triplicate.

2.8. Hemolytic activity

The hemolytic activity of the peptides was evaluated according to a previous method [41]. The sheep red blood cells (sRBCs) were washed twice with sterile PBS by centrifugation at 4000 rpm and 4 °C for 10 min. The sRBCs were resuspended in PBS and incubated with an equal volume of 2-fold diluted peptides in a 96-well plate for 1 h. sRBCs incubated with 1% Triton X-100 or PBS served as a positive and negative controls, respectively. Finally, the plate was centrifuged at 4000 rpm, 4 °C for 10 min, and the absorbance of the collected supernatant was measured at OD_{600}. All the tests were performed in triplicate.

2.9. Cytotoxicity toward eukaryotic cells

The cytotoxicity of the peptides toward HUVECs, BEAS-2B, L929, and L02 cell lines was assessed by the MTT assay. Cells in DMEM supplemented with 10% heat-inactivated FBS were seeded in a 96-well plate (approximately 1×10^4 cells/well for BEAS-2B and L02 cells and 7×10^3 cells/well for HUVECs and L929 cells) and cultured overnight at 37 °C, 5% CO_2. Subsequently, the cells were incubated in medium supplemented with 2-fold serial dilutions of peptides for 48 h. MTT solution was added to each well, and the plates were incubated for 4 h at 37 °C. After the supernatant was discarded, DMSO was added to dissolve the formazan, and the absorbance of each well was recorded at OD_{490}. All the tests were performed in triplicate.

2.10. Time-killing assay

A time-killing assay was performed as previously described [42]. Briefly, each bacterial strain at the logarithmic growth phase was collected by centrifugation and diluted with PBS to a density of 2×10^5 CFU/ml. Then, the bacterial suspension was incubated with the peptide or antibiotics at 4 ×MIC for a 5 ml coculture system (approximately 10^6 CFU) [38]. At the indicated time points (0, 0.5, 1, 2, 4, 8, 12, and 24 h), samples were removed and subjected to 10-fold serial dilution. Finally, the dilution plate method was used for bacterial counting. All the tests were repeated twice.

2.11. Live/dead cell staining assay

To investigate the protective effect of TS-CATH on infected cells, L929 cells were seeded in a 96-well plate at 2×10^4 cells/well and cultured overnight at 37 °C in a 5% CO_2 atmosphere for cell adherence. The clinical strain *E. coli* E24 was grown to the logarithmic growth phase, resuspended in DMEM, and adjusted to 2×10^8 CFU/ml for L929 cell infection at an MOI of 10:1. Subsequently, TS-CATH or ceftazidime was added at a final concentration of 4 ×MIC. In addition, L929 cells without infection served as controls, while infected L929 cells without drug treatment were used as a model. After coincubation at 37 °C in a 5% CO_2 atmosphere for 24 h, the cells were washed with PBS and stained with a calcein/PI live/dead assay kit (Beyotime Biotechnology, Shanghai, China). The stained cells were visualized under a Zeiss fluorescence microscope.

2.12. Stability analysis

The salt stability of the peptides was evaluated by the changes in peptide antibacterial activity at different salt concentrations [43]. The peptide stock solutions were 2-fold serially diluted from 128 to 0.5 μg/ml by MHB at 100, 150, or 200 mM NaCl, and the dilutions were inoculated in a 96-well plate. The test strains were cultured overnight at 37 °C to the logarithmic phase, and the bacteria were diluted to 2×10^5 CFU/ml by MHB at different salt concentrations. The bacterial suspensions were mixed with peptide dilutions (1:1, v:v) in a 96-well plate at the same NaCl concentration. The plate was incubated at 37 °C for 20 h, and MIC values were recorded as described above.

The thermal stability assessment was conducted by incubating the 1.024 mg/ml peptide at 37 °C, 60 °C, or 90 °C for 15 min. Aliquots of each sample were extracted, and MIC values were recorded as described above.

The serum stability experiment was performed in 25% mouse serum [44]. The peptide was incubated in 25% mouse serum at a final concentration of 1.024 mg/ml at 37 °C. Aliquots of the mixture (200 μl) were extracted periodically at 0, 0.5, 1, and 2 h for MIC detection as described above.

2.13. Protective effects of TS-CATH on E. coli-induced mouse bacteremia

ICR mice (5–6 weeks, SPF grade, half male and half female) were used to establish a bacteremia model by intraperitoneal (i.p.) injection of 500 μl (1×10^9 CFU/ml) of ceftazidime-resistant *E. coli* E24 isolates. At 2 h post bacterial inoculation, the mice were intraperitoneally injected with TS-CATH (10, 5, or 2.5 mg/kg, n = 12/group) or ceftazidime (5 mg/kg). Mice in the model group were injected with an equal volume of saline [42,45]. After 8 h of drug treatment (before the death of the model mice), three mice in each group were anesthetized with pentobarbital sodium (50 mg/kg, i.p.) and euthanized by the acute blood loss method to collect blood and count bacterial colonies in the blood, lung, spleen, kidney, and liver. Moreover, serum TNF-α, IL-1β, and IL-6 levels were detected by ELISA kits (MultiSciences Biotech, Hangzhou, China). Routine H&E staining was performed to observe pathological changes in the lung tissues of *E. coli* E24-infected mice. The survival and weight of the remaining mice were monitored daily for up to 7 days.

2.14. Preparation of the TS-CATH hydrogel

TS-CATH was precisely weighed and mixed with 400 mg of glycerol and 3 g of deionized water. Subsequently, 70 mg of methyl cellulose was slowly added with stirring. Deionized water was then added to reach a total weight of 4 g, followed by incubation at 4 °C for swelling. To remove the bubbles, the hydrogel was centrifuged at 3000 rpm for 3 min. Finally, TS-CATH hydrogels with concentrations of 0.125%, 0.25%, and 0.5% (w/w) were obtained, which demonstrated excellent stability, retaining over 80% of its activity after being stored at 4 °C for one year (data not shown). Similarly, hydrogels without peptides were also prepared.

2.15. Protective effects of TS-CATH on P. aeruginosa-induced skin wound infection

For bacterial skin infection, ICR mice were anesthetized with pentobarbital sodium (50 mg/kg, i.p.), and a full-thickness skin wound was created on the dorsal skin using a biopsy puncher with a diameter of 1 cm. The wounds were infected with 20 μl (5×10^8 CFU/ml) of meropenem-resistant *P. aeruginosa* P1, and a gentle stream of air was applied to the inoculation site until the skin appeared wet but with no standing volume from the inoculum suspension. After 0.5 h, the wounds (n = 9 per group) were topically treated with the hydrogels. For model mice, hydrogels without peptides were used. For TS-CATH-treated mice, 0.125% (2.5 mg/kg), 0.25% (5 mg/kg), or 0.5% (10 mg/kg) TS-CATH hydrogels were administered. For mice in the control groups, meropenem (40 mg/kg) dissolved in saline or ointment containing the compound polymyxin B (40 mg/kg) was applied. All drugs were administrated every two days for 13 days. Each group was housed separately to avoid cross-contamination. The wounds were photographed at the indicated time points, and wound sizes were determined using ImageJ. On days 3 and 7, the bacterial counts of the wound specimens were recorded, and the wound specimens were collected for H&E and Masson staining.

2.16. Cell scratch assay

L929 cells, which are usually used to study cell migration via scratch assays [46,47], were resuspended at 2×10^5 cells/ml in DMEM supplemented with 10% heat-inactivated FBS, seeded into 12-well plates, and cultured overnight for attachment. A pipette was used to penetrate the cell layer, and cell scratches were created. TS-CATH at final concentrations of 4, 8, and 16 μg/ml was added, and blank controls without drug treatment were used. The 12-well plates were placed in an incubator containing 5% CO_2 at 37 °C and were removed and photographed under a microscope at 0 h and 48 h to observe the migration of the scratched cells. Five photos of cell scratches were randomly selected from each group, and the scratch area was calculated using ImageJ software.

2.17. Zeta potential detection

The clinical strains *E. coli* E24 and *P. aeruginosa* P1 were cultured overnight in MHB and washed twice with deionized water by centrifugation (10,000 rpm, 5 min). Bacteria were resuspended in deionized water at 2×10^8 CFU/ml and treated with TS-CATH at final concentrations of 2, 4, 8, and 16 μg/ml. Bacteria not treated with TS-CATH served as control. The zeta potentials of the bacteria were obtained with a zeta potential and particle size analyzer (Brookhaven Instruments Corporation, Austin, Texas, USA) [45]. All the tests were performed in triplicate.

2.18. NPN uptake assay

An N-phenyl-1-naphthylamine (NPN) probe uptake assay was performed as previously described with minor modifications [48]. The clinical strains *E. coli* E24 and *P. aeruginosa* P1 were resuspended in HEPES (containing 0.2% glucose, pH 7.4) at 2×10^8 CFU/ml and the fluorescent probe NPN (Aladdin, Shanghai, China) was added at a final concentration of 10 μM. The mixture was incubated with 2-fold serial dilutions of TS-CATH in a black 96-well plate, and polymyxin B (8 μg/ml) was used as a positive control. The time-dependent effect of TS-CATH on NPN fluorescence (λ excitation = 350 nm, λ emission = 420 nm) was recorded. All the tests were performed in triplicate.

2.19. PI uptake assay

The clinical strains *E. coli* E24 and *P. aeruginosa* P1 were resuspended in saline at 2×10^8 CFU/ml, and the fluorescent probe PI (Sigma—Aldrich, USA) was added at a final concentration of 40 μg/ml. The mixture was incubated with 2-fold serial dilutions of TS-CATH in a black 96-well plate. The time-dependent effect of TS-CATH on PI fluorescence (λ excitation = 535 nm, λ emission = 615 nm) was periodically recorded by a microplate reader. All the tests were performed in triplicate.

2.20. ONPG assay

The clinical strain *E. coli* E24 at the logarithmic growth phase was washed twice with saline by centrifuging at 10,000 rpm for 5 min and resuspended in HEPES (containing 40 mM glucose, pH 7.4) at 2×10^8 CFU/ml. ONPG (Aladdin, Shanghai, China) was added at a final concentration of 1.5 mM. The mixture was incubated with 2-fold serial dilutions of TS-CATH in a 96-well plate, and the optical density was recorded periodically at 420 nm. All the tests were performed in triplicate.

2.21. TEM characterization

The morphological changes of bacteria treated with peptide were observed via TEM [45]. *E. coli* E24 and *P. aeruginosa* P1 (5×10^8 CFU/ml) at the logarithmic growth phase were incubated with TS-CATH at 4 ×MIC (16 μg/ml) for 40 min to achieve maximum membrane damage, and the untreated bacteria were used as the negative controls. After centrifugation, the bacteria were resuspended in electron microscope fixative and then suspended in 1% agarose. Subsequently, bacteria were fixed with 1% OsO_4, followed by resin penetration and embedding. The samples were then polymerized at 65 °C for 48 h. Ultrathin sections were prepared and stained with a 2% uranium acetate-saturated alcohol solution. Finally, images were captured using an HT7800 transmission electron microscope (Hitachi, Japan).

2.22. Bacterial membrane potential changes

DiSC3(5) was used to characterize the changes in bacterial membrane potential following exposure to AMPs as described previously [49]. That is, the clinical strains *E. coli* E24 and *P. aeruginosa* P1 were cultured overnight and washed twice with saline. Bacteria were resuspended in HEPES buffer (10 mM, 20 mM glucose, 0.1 M KCl, pH 7.4) at 2×10^7 CFU/ml. Subsequently, a final concentration of 0.2 mM EDTA and 4 μM DiSC3(5) (Macklin, Shanghai, China) were added. The bacterial inoculum was incubated in a dark environment for 30 min at 37 °C. Finally, TS-CATH or melittin was added to each well at the indicated concentrations, and the fluorescence (λ excitation = 622 nm, λ emission = 670 nm) was recorded every minute by a microplate reader. All the tests were performed in triplicate.

2.23. Bacterial ATP level assay

A BacTiter-Glo™ Microbial Cell Viability Kit (Promega, USA) was used to measure the microbial ATP levels at the indicated time points. After equilibration to room temperature, BacTiter-Glo™ Reagent was

prepared by mixing BacTiter-Glo™ Substrate with BacTiter-Glo™ Buffer. The clinical strains *E. coli* E24 and *P. aeruginosa* P1 were cultured overnight and washed twice with saline. Bacteria were resuspended in MHB at 1×10^8 CFU/ml and divided into six groups. The aliquots were added to TS-CATH solution at final concentrations of 0, 0.5, 1, 2, or 4 μg/ml. Carbonyl cyanide m-chlorophenylhydrazone (CCCP) (Aladdin, Shanghai, China) at 8 μg/ml was used as the positive control, and MHB served only to eliminate background interference. After 0, 1, 2, 3, or 4 h of incubation at 37 °C, 50 μl of each group was inoculated into a white 96-well plate, and 50 μl of BacTiter-Glo™ Reagent was added. The luminescence intensity was detected by a microplate reader within 5 min. All the tests were performed in triplicate.

2.24. Resazurin assay

The clinical strains *E. coli* E24 and *P. aeruginosa* P1 were resuspended in MHB at 1×10^8 CFU/ml, and resazurin (Aladdin, Shanghai, China) was added (at a final concentration of 0.1 mg/ml). The mixture was incubated with 2-fold serial dilutions of TS-CATH in a black 96-well plate. The time-dependent effect of fluorescence (λ excitation = 550 nm, λ emission = 590 nm) was recorded every 10 min over 2.5 h by a microplate reader periodically. All the tests were performed in triplicate.

2.25. Respiratory chain dehydrogenase enzyme activity assay

2,3,5-Triphenyltetrazolium chloride (TTC), an electron acceptor, was used to evaluate respiratory chain dehydrogenase activity [50,51]. The clinical strains *E. coli* E24 and *P. aeruginosa* P1 were cultured overnight and washed twice with saline by centrifuging at 10,000 rpm for 5 min. Bacteria were resuspended in Tris-HCl buffer (0.05 mol/L, glucose 0.1 mol/L, pH 8.6) at 5×10^8 CFU/ml, and TTC (Macklin, Shanghai, China) was added at a final concentration of 0.25 mg/ml. This mixture was divided into seven groups, and aliquots were added to TS-CATH solution at final concentrations of 0, 0.5, 1, 2, 4, 8, and 16 μg/ml. After 1 h of incubation at 37 °C, the reaction was terminated by adding 100 μl of sulfuric acid, followed by the addition of n-butanol (1:4, v:v). After mixing and incubating for 10 min, the aliquots were centrifuged at 4000 rpm for another 5 min. The supernatant was carefully removed and added to a 96-well plate, after which the absorbance at 490 nm was measured. All the tests were performed in triplicate.

2.26. DNA binding assay

A DNA binding assay was performed by gel retardation experiments as described previously [52]. Bacterial genomic DNA was extracted from *E. coli* E24 and *P. aeruginosa* P1 using a Bacteria Genomic DNA Kit (CWBIO, Jiangsu, China). DNA samples (150 μg/ml, 5 μl) were mixed with equal volumes of TS-CATH to achieve final concentrations of 2, 4, 8, and 16 μg/ml TS-CATH. After 10 min of incubation at 25 °C, 1% agarose gel electrophoresis was performed to detect the migration of DNA in the different groups. This experiment was repeated twice.

2.27. ROS measurement

The ROS probe DCFH-DA was utilized to assess ROS levels in bacteria as previously described with some modifications [53]. The clinical strain *E. coli* E24 was cultured overnight to the logarithmic phase and then washed twice with saline by centrifuging at 10,000 rpm for 5 min. Bacteria were resuspended in PBS (containing 2% glucose) at 1×10^8 CFU/ml, and DCFH-DA (Aladdin, Shanghai, China) was added at a final concentration of 10 μM. After incubating at 37 °C for 20 min, the mixture was centrifuged and resuspended in PBS to remove the free DCFH-DA. Subsequently, the mixture was incubated with 2-fold serial dilutions of TS-CATH, 2 μg/ml polymyxin B, 0.15% H_2O_2 (positive control), and 4 μg/ml TS-CATH with an ROS scavenger (1 mg/ml NAC) or inhibitor (10 μg/ml DP, 1 mg/ml TU) (Aladdin, Shanghai, China) in a black 96-well plate. The time-dependent effect of TS-CATH on DCF fluorescence (λ excitation = 488 nm, λ emission = 525 nm) was periodically recorded every 15 min by a microplate reader. All the tests were performed in triplicate.

2.28. RT—PCR

The clinical strain *E. coli* E24 was cultured overnight at 37 °C and adjusted to 1×10^8 CFU/ml with MHB. Bacterial suspensions were cultured with 2 μg/ml (sub-MIC) TS-CATH for 0, 0.5 and 1 h. Bacterial total RNA was extracted with RNA-Easy Isolation Reagent (Vazyme, Nanjing, China). Residual DNA was digested with a gDNA digester mix kit (Yeasen, Shanghai, China), and cDNAs were synthesized using SuperMix (Yeasen, Shanghai, China). Target gene expression was measured with a SYBR Green Master Mix kit (Yeasen, Shanghai, China). All primers used for RT—PCR are listed in Table S8. The gene expression levels were calculated by the ΔΔCt method after normalization to the 16 S ribosomal gene *rsmA* (a housekeeping gene known as *ksgA*) levels [54,55]. All the tests were performed in triplicate.

2.29. Statistical analysis

Assay results were subjected to statistical analysis using the GraphPad Prism software package. One-way analysis of variance (ANOVA) or Student's t test with three or more replicates was applied. Differences with $p < 0.05$ were considered statistically significant. Error bars represent the standard error of the mean.

3. Results

3.1. Identification and characterization of TS-CATH, BM-CATH, and LV-CATH

Three novel cathelicidin family antimicrobial peptides from different species were obtained by screening and BLAST against the *Thamnophis sirtalis*, *Balaenoptera musculus*, and *Lipotes vexillifer* NCBI protein databases (Fig. 1A). Several cathelicidin-related protein precursors were obtained (Fig. S1), and the mature peptide regions were characterized (Table S1). The representative peptides of each species were screened out by their physicochemical properties via multisequence alignment, which revealed that the sequence compositions were similar to those of other representative cathelicidin precursors (Fig. 1B); these peptides included a signal peptide at the N-terminus, a conserved cathelin domain with four invariantly spaced cysteines, and a mature antimicrobial peptide with various sequences at the C-terminus. The truncated mature peptides from *Thamnophis sirtalis*, *Balaenoptera musculus*, and *Lipotes vexillifer* were named TS-CATH, BM-CATH, and LV-CATH (Fig. 1C–E), respectively, and were subsequently synthesized for analysis of their structural properties and activities.

The three novel cathelicidin antimicrobial peptides feature typical cationic, amphiphilic, and α-helical properties. The three-dimensional model structures of the peptides predicted by SWISS-MODEL show that the three peptides adopt highly α-helical conformations mainly distributed at their N-terminal. Moreover, cationic residues or hydrophobic residues are assembled relatively at the opposite face of the α-helix, forming hydrophilic and hydrophobic faces, respectively, suggesting the key property of amphiphilicity. Similar results were obtained by helical wheel projection (Fig. 1F–H) and CD analysis (Fig. 1I–K). The CD spectra of the chemically synthesized peptides revealed a strong positive peak at 190 nm and two negative peaks near 208 nm and 220 nm, indicating the presence of an α-helix in 25 mM SDS, while a negative peak near 200 nm represented a random coil structure in water. The helical properties of the peptides were predicted and presented by helical wheel projections. As shown in Fig. 1F–H, the helical wheel diagrams of peptides illustrate the assembly level of cationic or hydrophobic residues alongside their corresponding amino acid

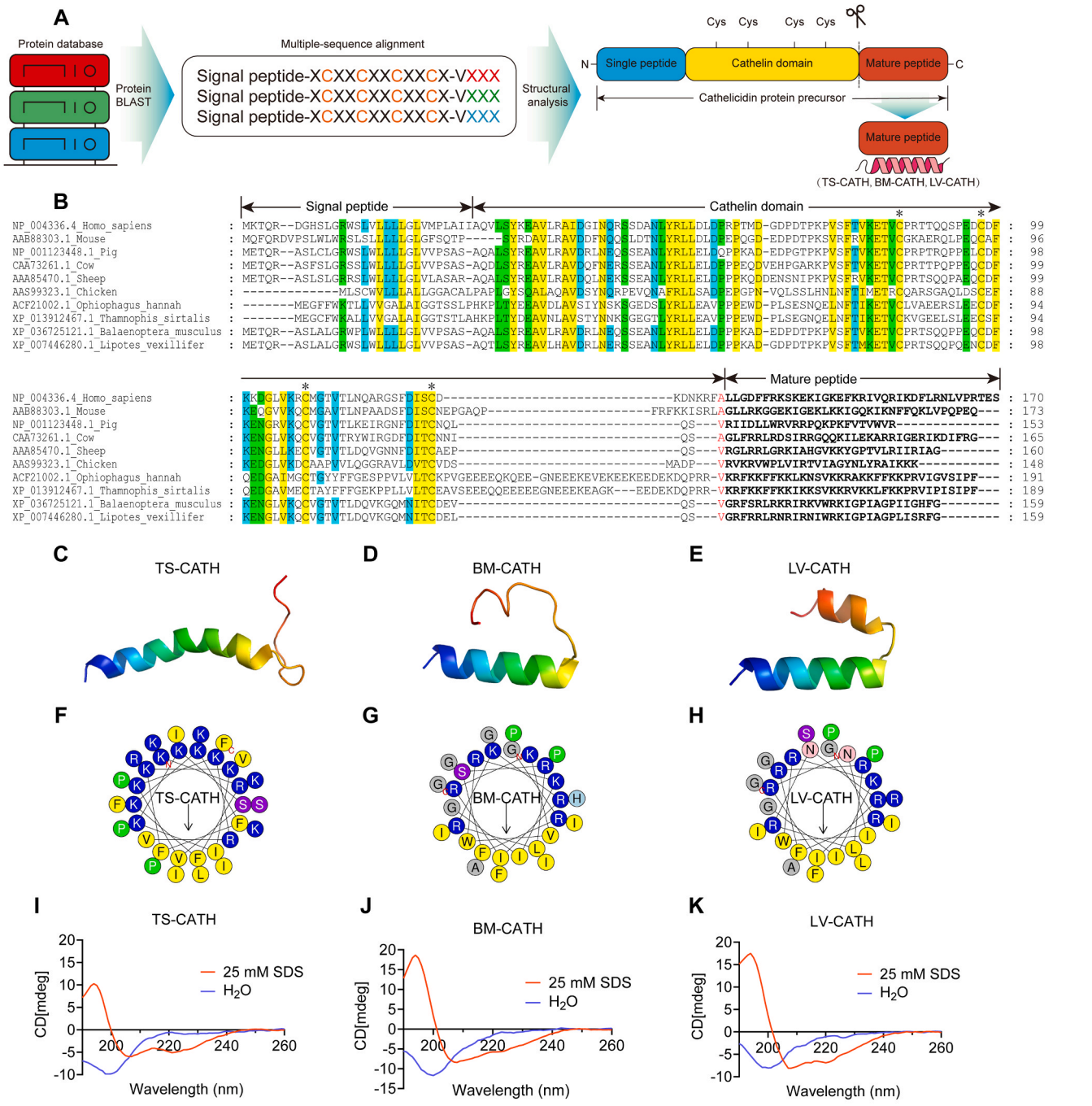

L

Peptide	Sequence	H	μH	Z	L	Mw
TS-CATH	KRFKKFFKKIKKSVKKRVKKLFKKPRVIPISIPF	0.226	0.474	16	34	4217.36
BM-CATH	GRFSRLRKRIRKVWRKIGPIAGPIIGHFG	0.364	0.547	9	29	3373.06
LV-CATH	GRFRRLRNRIRNIWRKIGPIAGPLISRFG	0.333	0.555	9	29	3477.13

Fig. 1. Structures and properties of novel cathelicidin antimicrobial peptides. (A) Schematic diagram illustrating the procedure for identifying novel cathelicidin antimicrobial peptides. (B) Multisequence alignment of TS-CATH, BM-CATH, and LV-CATH precursors with other representative cathelicidins by MEGA 7. The conserved residues are shaded, and the conserved residues in the cathelin domain are indicated with asterisks. 3D structures of (C) TS-CATH, (D) BM-CATH, and (E) LV-CATH predicted by SWISS-MODEL. (F–H) Helical wheel projections of TS-CATH, BM-CATH, and LV-CATH, respectively. (I–K) CD spectra for the secondary structures of the peptides in water and 25 mM SDS. (L) Physicochemical properties. H: Hydrophobicity; μH: Hydrophobic moment; Z: Net Charges; L: Length; MW: Molecular Weight.

residues. These diagrams reveal characteristic amphipathic structures, where the hydrophilic face is formed by cationic residues such as Lys and Arg pointing upward, while the hydrophobic face is constructed by hydrophobic residues such as Phe, Ile, Leu, and Trp facing downward. However, TS-CATH retains more cationic residues with a net charge of + 16, although the hydrophobic moment and hydrophobicity are lower than those of BM-CATH or LV-CATH (Fig. 1L). Collectively, the data gathered demonstrate that the three novel cathelicidin antimicrobial

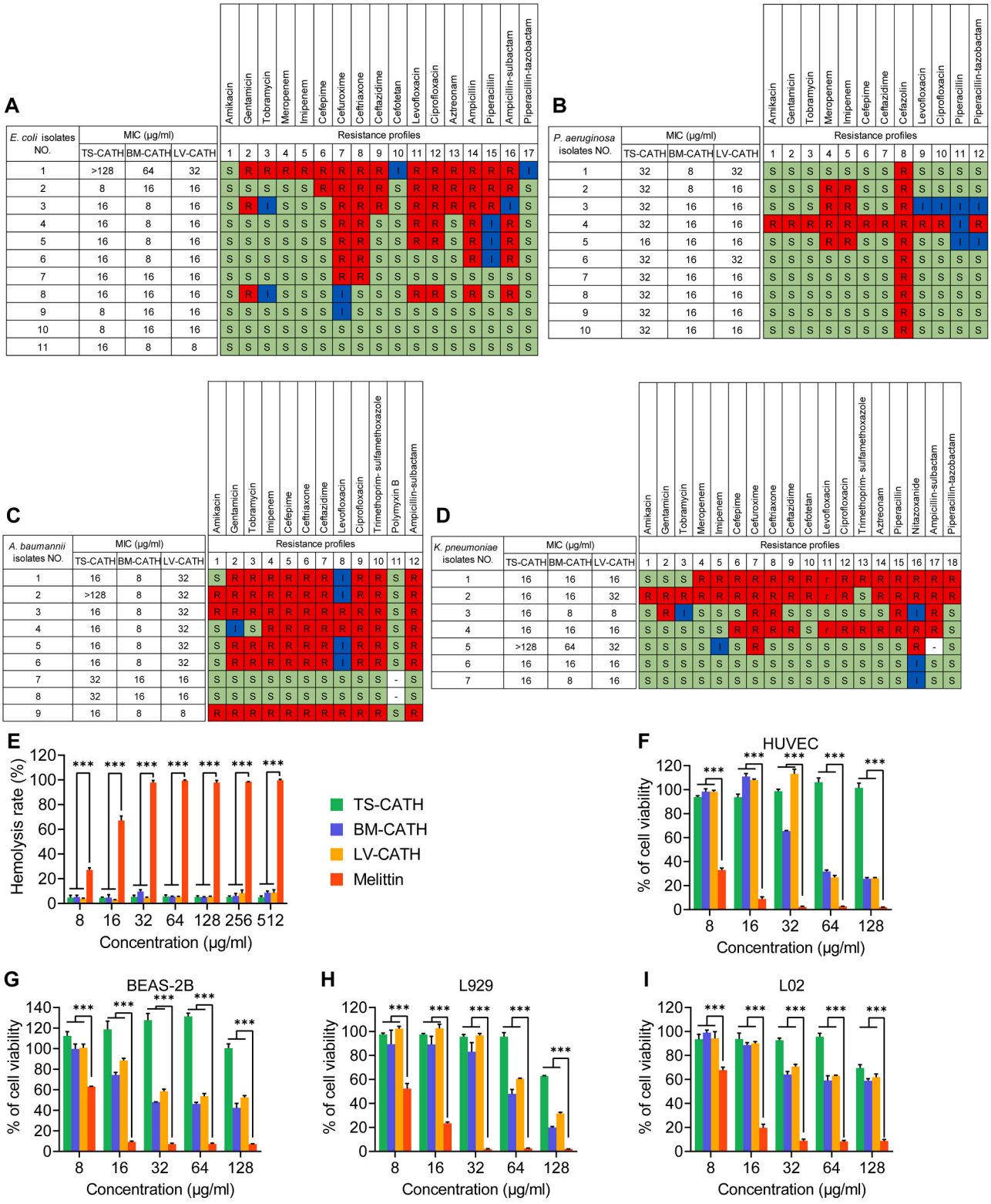

Fig. 2. Bioactivity of novel cathelicidin antimicrobial peptides. (A–D) Antimicrobial activity against clinically isolated *E. coli*, *P. aeruginosa*, *A. baumannii* and *K. pneumoniae*. The MICs were determined by the agar dilution assay issued by CLSI. (E) Hemolytic activity toward sRBCs and (F–I) cytotoxicity toward mammalian cells, including HUVECs, BEAS-2B cells, L929 cells, and L02 cells. Statistical analyses were performed using a two-tailed Student's t test. * $P < 0.05$, * * $P < 0.01$, * ** $P < 0.001$, and ns, not significant. The data are presented as the means ± SDs.

peptides exhibit an α-helical conformation, abundant cationic residues, and appropriate amphiphilic properties. These properties indicate that these sequences have potential antimicrobial activity.

3.2. Functional screening of peptides based on antimicrobial activity and cytotoxicity

To identify peptides with the potential to effectively eliminate drug-resistant pathogens with low cytotoxicity, an agar dilution assay was performed to determine the MICs, and an MTT assay was applied to evaluate cell viability after peptide treatment. As shown in Fig. 2A–D, the three novel peptides possessed broad-spectrum antimicrobial activity. BM-CATH displayed potent bactericidal activity against gram-negative bacteria, with MICs ranging primarily from 8–16 μg/ml, surpassing those of LV-CATH, which had MICs ranging from 8–32 μg/ml. TS-CATH demonstrated comparable antimicrobial activity against gram-negative bacteria, with MICs range mostly spanning 8–32 μg/ml, paralleling the performance of LV-CATH. The MICs against the ATCC standard strains were measured by the same method (Table S4).

Importantly, most of the clinically sensitive and β-lactam-resistant strains of *E. coli* were sensitive to all three peptides, with MICs ranging from 8–16 μg/ml (Fig. 2A). There was no significant difference in the susceptibility of the peptides to clinically sensitive or carbapenem-resistant *P. aeruginosa*, with most of the MICs being 32 μg/ml for TS-CATH and 16 μg/ml for BM-CATH and LV-CATH (Fig. 2B). Multidrug-resistant *A. baumannii* is encountered quite commonly in clinical treatment. As shown in Fig. 2C, for clinically antibiotic-sensitive and clinical *A. baumannii* strains resistant to cephalosporins, carbapenems, β-lactamase inhibitors, and fluoroquinolones, the MICs of BM-CATH were maintained at 8–16 μg/ml, and the MICs of TS-CATH and LV-CATH mostly ranged from 16–32 μg/ml. Except for *K. pneumoniae* 5#, the MICs of the three peptides varied slightly against *K. pneumoniae* isolates, with a concentration of approximately 16 μg/ml (Fig. 2D).

The three peptides exhibited negligible hemolytic activity toward sRBCs (Fig. 2E), showing $< 10\%$ hemolysis even at the highest screened concentration (512 μg/ml). The cytotoxicity of the peptides toward HUVEC, BEAS-2B, L929, and L02 cells was also evaluated (Fig. 2F–I). Compared with BM-CATH and LV-CATH, TS-CATH exhibited less cytotoxicity toward BEAS-2B cells and HUVECs at 128 μg/ml or toward L929 and L02 cells at 64 μg/ml, with IC_{50} values > 128 μg/ml against all four cell lines.

In summary, our data indicate that these three peptides exhibit robust broad-spectrum antibacterial activity and negligible sheep red blood cell hemolysis, with undetectable cytotoxicity at bactericidal concentrations. Notably, TS-CATH was selected for further investigation of its antibacterial potential *in vitro* and *in vivo*, as well as its bactericidal mechanism, given its exceptional antimicrobial activity against gram-negative bacteria and minimal cytotoxicity.

3.3. TS-CATH exhibits effective and rapid bactericidal activity against drug-resistant pathogens in vitro

To further explore the antimicrobial spectrum and bactericidal activity of TS-CATH, the MICs and MBCs against clinically isolated drug-resistant strains were detected by a broth microdilution assay (Table S2). Indeed, the MICs of TS-CATH against clinical isolates of *E. coli*, *P. aeruginosa*, *K. pneumoniae,* and *A. baumannii* were all 4 μg/ml, and TS-CATH could completely kill all of the bacteria at 16 μg/ml (4 ×MIC), and some of them even had MBCs of 8 μg/ml (2 ×MIC) or 4 μg/ml. Moreover, TS-CATH also showed bactericidal activity against *H. pylori* SS1 at an MIC of 4 μg/ml. Nonetheless, the MICs of TS-CATH against *S. aureus* and MRSA reached 16 μg/ml, and there was no significant inhibitory effect on the growth of the fungi.

TS-CATH exhibited a rapid killing effect against drug-resistant strains of *E. coli*, *P. aeruginosa,* and *K. pneumoniae* and could eradicate bacteria within 0.5 h at 16 μg/ml (Fig. 3A–F). In contrast to TS-CATH, ceftazidime at 64 μg/ml required 12 h to completely kill *E. coli* (Fig. 3A), and meropenem at 32 μg/ml required 8 h to kill *P. aeruginosa* (Fig. 3C). Moreover, *K. pneumoniae*, which was eliminated within 4 h, required 512 μg/ml ceftazidime (Fig. 3E). To further explore the bactericidal kinetics of TS-CATH, the bactericidal curves against clinical isolates within 0.5 h were determined. Notably, after TS-CATH was added, the number of tested gram-negative bacteria decreased by more than 3 log CFU, indicating that 99.9% of the bacteria were killed within 2 min (Fig. 3B) and that *P. aeruginosa*, *E. coli*, and *K. pneumoniae* were effectively killed within 5, 10, and 20 min (Fig. 3D and F). The selective killing activity of TS-CATH against bacteria rather than normal cells was assessed by the protection of L929 cells infected with ceftazidime-resistant *E. coli* (Fig. 3G). After 24 h of infection, all the L929 cells were dead and stained red according to the Live/Dead Kit. Although the addition of 16 μg/ml ceftazidime successfully inhibited bacterial growth, it also induced damage to the cocultured L929 cells. Taken together, these results indicate that TS-CATH has excellent antibacterial and bactericidal effects against all drug-resistant gram-negative bacteria and has a rapid killing effect *in vitro*.

3.4. TS-CATH effectively protected mice against ceftazidime-resistant E. coli-induced acute systemic infection

A mouse bacteremia model was established by intraperitoneal injection of a minimal lethal dose of ceftazidime-resistant *E. coli* (Fig. 4A), which caused 100% mouse death on the first day postinfection and led to the loss of 85.7% of the mice treated with 5 mg/kg ceftazidime. Remarkably, seven days after infection, 10 mg/kg TS-CATH rescued 85.7% of the mice, and even 2.5 mg/kg TS-CATH had stronger protective effects than did ceftazidime (5 mg/kg) *in vivo* (Fig. 4B). In addition, the body weights of the mice in all the groups decreased on the first day after infection (Fig. 4C). However, TS-CATH increased the body weights of the mice in a dose-dependent manner after the second day post infection. Furthermore, the ability of TS-CATH to eliminate *E. coli* in infected mice was determined by counting bacterial colonies in blood and organs (Fig. 4D–I). The mice in the model group responded the same as those in the ceftazidime-treated group, with approximately 1×10^9 CFU/g in the lung, liver, spleen, and kidney tissues and 1×10^9 CFU/ml in the blood, suggesting that 5 mg/kg ceftazidime failed to kill *E. coli in vivo* . In contrast, TS-CATH treatment significantly decreased the bacterial counts in each tissue and blood sample. Compared with those in the model and ceftazidime-treated groups, TS-CATH at 10 and 5 mg/kg dramatically reduced the bacterial load to 10^5 CFU/ml, a decrease of 4 log CFU in blood, with a similar reduction to 10^6 or 10^5 CFU/ml in organs. Treatment of mice with peptide significantly reduced the number of bacterial colonies in the tissues, while there was no significant difference in the bacterial load between the ceftazidime-treated and untreated mice.

The overproduction of proinflammatory cytokines, such as IL-1β, TNF-α, and IL-6, followed by infection tends to induce severe injury to tissues. Serum samples from each group were collected after 8 h of infection and used to measure the levels of proinflammatory cytokines via an ELISA kit. Compared with those in the model group, the *E. coli*-induced secretion levels of TNF-α, IL-1β, and IL-6 in the serum were markedly and dose-dependently attenuated by TS-CATH (Fig. 4J–L), while the administration of ceftazidime had little effect on the secretion of these cytokines. H&E staining of lung tissue from the normal group clearly revealed alveolar and bronchial branches and interstitial structures. However, the lung tissues of the model and ceftazidime-treated groups exhibited drastic inflammatory cell infiltration, alveolar wall thickening, adjacent alveolar space enlargement, and local hemorrhage (Fig. 4M). Notably, the inflammatory infiltration and bleeding in the lung tissues of the mice treated with TS-CATH were alleviated, indicating that the peptides could significantly reduce the lung tissue injury caused by bacterial infection.

These data indicate that TS-CATH can significantly improve the

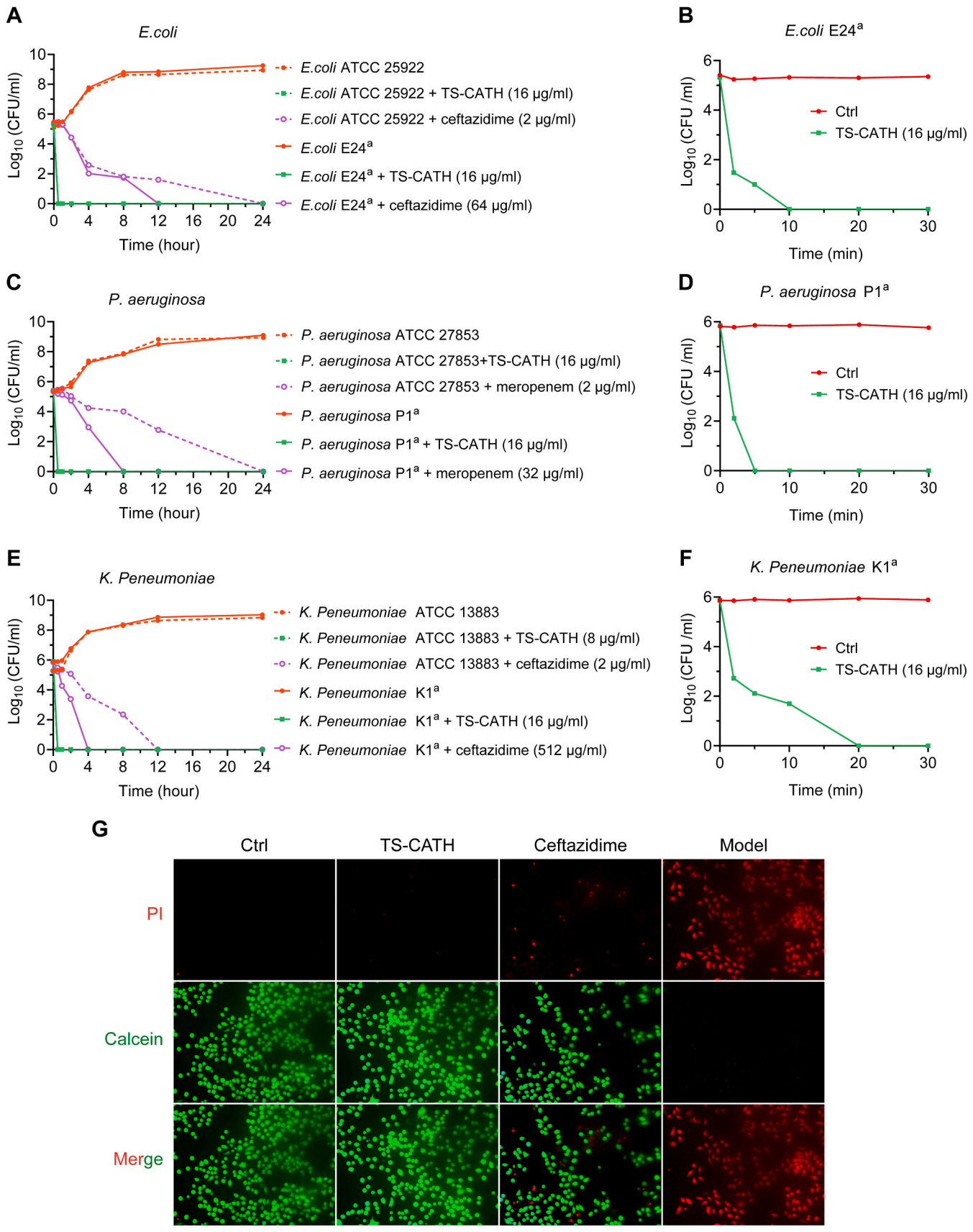

Fig. 3. Killing curves of TS-CATH and its selective toxicity against clinically gram-negative bacteria. TS-CATH rapidly kills clinically isolated drug-resistant strains, including (A–B) *E. coli*, (C–D) *P. aeruginosa*, and (E–F) *K. pneumoniae*. a: Clinically isolated strains. (G) Calcein/PI live/dead cell staining of L929 cells infected with *E. coli* and TS-CATH selective toxicity against *E. coli* E24 and protection of L929 cells from bacterial infection.

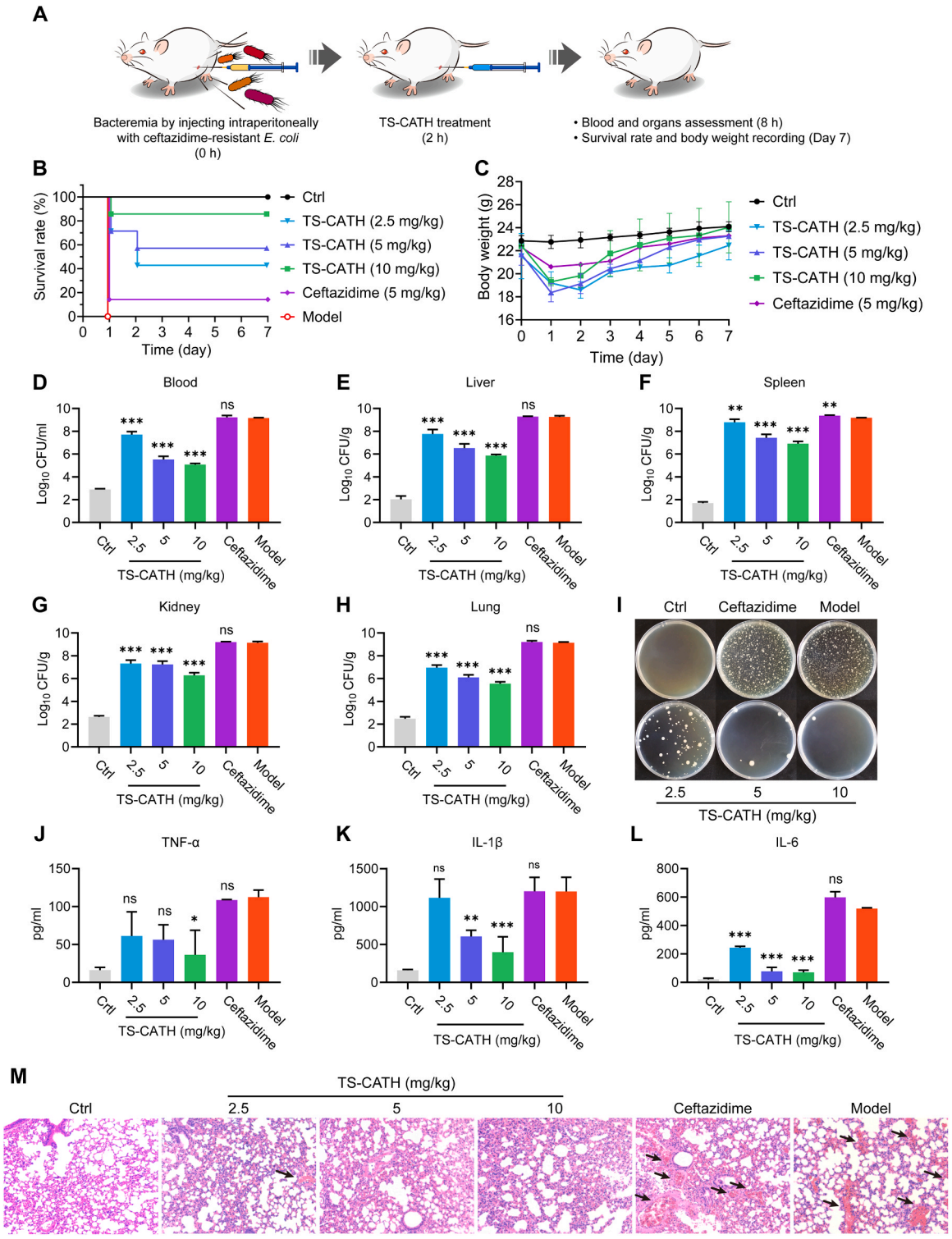

Fig. 4. TS-CATH protected mice against drug-resistant resistant *E. coli*-induced acute systemic infection. (A) Schematic diagram illustrating the timeline of the experimental process. (B) Survival rates and (C) body weights of mice inoculated via intraperitoneal injection of the minimum lethal dose of *E. coli* (1×10^9 CFU/ml) and treated with TS-CATH (2.5, 5, or 10 mg/kg) or ceftazidime (5 mg/kg). (D–H) Bacterial counts in mouse lung, liver, spleen, kidney, and blood and (I) photographs of agar plates of lung samples. (J–L) ELISA analysis of the serum levels of TNF-α, IL-1β, and IL-6 in mice at 8 h after infection. (M) H&E staining (×100) of mouse lungs. Black arrows: lung lesions. The data are presented as the means ± SDs. Statistical analyses were performed using one-way ANOVA (C-G, I-K). * $P < 0.05$, * * $P < 0.01$, * ** $P < 0.001$, and ns, not significant, compared with the model. The data are presented as the means ± SDs.

survival rate of ceftazidime-resistant *E. coli*-infected mice in a dose-dependent manner and has a protective effect on the maintenance of body weight.

3.5. TS-CATH significantly ameliorated skin wound infection induced by drug-resistant P. aeruginosa

Hydrogels are easy to spread and comfortable, can absorb tissue

exudate, do not interfere with the normal physiological effects of the skin, have a certain water retention effect, and can promote the transdermal absorption of drugs [56,57]. A mouse model of full-thickness skin damage caused by infection with *P. aeruginosa* was generated to further evaluate the therapeutic efficacy of the TS-CATH hydrogels (Fig. 5B). The process of wound healing was recorded, as shown in Fig. 5A, and the results were quantitatively analyzed, as shown in Fig. 5C. Notably, the 10 mg/kg TS-CATH hydrogel promoted wound healing within 13 days, and the healing speed was also similar to those of the positive control groups treated with meropenem (40 mg/kg) and polymyxin B (40 mg/kg). However, medium-dose (5 mg/kg) and low-dose (2.5 mg/kg) TS-CATH hydrogels had limited effects on wound closure, and the wound area appeared the same as that of the model group, which still had scabs on the 13th day.

Moreover, to evaluate the ability of TS-CATH hydrogels to eliminate *P. aeruginosa* colonization in wound tissues, the number of bacterial colonies was determined by counting viable bacteria on the 3rd day (Fig. 5E) and 7th day (Fig. 5D and F). Treatment with TS-CATH hydrogels dose-dependently reduced the number of bacterial colonies in the skin tissue, and this clearance effect was more pronounced on the 7th day (Fig. 5F), with a 40-fold reduction in the number of bacterial colonies after treatment with 10 mg/kg TS-CATH hydrogels compared with that in the model group.

Furthermore, H&E and Masson staining were utilized to assess injuries, inflammatory reactions, and collagen regulation in skin wound tissues collected on the 7th day. The skin of the mice in the model group was edematous, which was accompanied by inflammatory cell infiltration and fibroblast proliferation (Fig. 5H). Although enlarged blood vessels were also observed in the medium- and low-dose TS-CATH-treated groups, no substantial inflammatory cell infiltration was observed. Indeed, wound skin treated with medium- or high-dose TS-CATH displayed a clear epidermal structure with more hair follicles, sweat glands and collagen deposited in dermal tissue (Fig. 5H and I). Full-thickness skin excision invariably results in the formation of scar tissue that lacks miniature organ structures such as hair follicles [58]. However, the presence of regenerated hair follicles in the TS-CATH hydrogel treatment groups indicated that this hydrogel has the potential to promote scarless repair. L929 cells are mouse fibroblasts that were used to study cell migration via the scratch assay method *in vitro* [46,47], and the cell scratch assay results also indicated that TS-CATH could improve the motility of L929 cells (Fig. 5G). These results demonstrated that TS-CATH can ameliorate wound infection and improve wound closure.

3.6. TS-CATH induced disruption of the bacterial membrane

Positively charged peptides can directly bind to negatively charged groups on the surface of bacteria, which is the basis for the antibacterial activity of cationic antimicrobial peptides [59]. A particle size potentiometer was used to detect changes in the bacterial surface potential after the addition of TS-CATH. As shown in Fig. 6A, the positively charged peptide TS-CATH reduced the negative surface charges of *E. coli* E24 and *P. aeruginosa* P1 in a dose-dependent manner. When the peptide concentration was 16 μg/ml (4 ×MIC), the surface negative potential of *E. coli* decreased from − 31.4 mV to − 1.1 mV (Fig. 6B), indicating that the cationic peptide TS-CATH that accumulated on the surface of bacteria could neutralize the negative surface charge of bacteria and bind to bacteria via electrostatic interactions.

NPN is a fluorescent probe that detects hydrophobicity and can enter the exposed hydrophobic phospholipid layer inside disrupted bacterial outer membranes to generate a fluorescence signal upon excitation. The NPN uptake results showed that the peptide TS-CATH increased the fluorescence intensity of NPN in a dose-dependent manner (Fig. 6C and D). When the peptide concentration reached 8 μg/ml, the fluorescence intensity of NPN was the same as that of 10 μg/ml polymyxin B, and the increase in TS-CATH concentration did not further increase the fluorescence intensity of NPN, suggesting that TS-CATH at 8 μg/ml could maximize the damage to the bacterial outer membranes of *E. coli* E24 and *P. aeruginosa* P1.

The ability of bacteria to uptake PI dye, which cannot penetrate intact bacterial cell membranes, was detected to explore the degree of bacterial cell membrane damage. The addition of TS-CATH dose-dependently enhanced the fluorescence intensity of the PI dye, indicating destruction of the bacterial inner membrane (Fig. 6E and F).

β-galactosidase decomposes o-nitrophenyl-β-D-galactoside pyranoside (ONPG) to produce galactose and yellow 2-nitrophenol, which can be detected at an absorbance of 420 nm. The leakage of bacterial contents is demonstrated by the decomposition of ONPG in the solution resulting from the release of β-galactosidase from the cell due to the rupture of the bacterial cell membrane. The addition of TS-CATH promoted dose- and time-dependent increases in absorbance, suggesting that TS-CATH can disrupt the bacterial cell membrane and cause the efflux of bacterial contents (Fig. 6G).

TEM was performed to observe the changes in the internal or external morphology of *E. coli* E24 and *P. aeruginosa* P1 after TS-CATH treatment. In the absence of TS-CATH, *E. coli* maintained a smooth surface, intact bacterial cell wall structure, and intact cytoplasm. Remarkably, in the presence of TS-CATH, *E. coli* cells had incomplete cell walls with multiple holes, leakage of cytoplasmic contents, and vacuolization, with a similar phenomenon observed for *P. aeruginosa* P1 treated with TS-CATH (Fig. 6H). These observations further indicated that the overwhelming cell wall and membrane disruption induced by TS-CATH resulted in bacterial death.

DiSC3(5) is a membrane potential-sensitive probe that emits fluorescence when the transmembrane potential is depolarized. Considering the above finding that TS-CATH could induce bacterial cell membrane permeation, DiSC3(5) was used to explore whether TS-CATH could reduce the membrane potential. The changes in the fluorescence intensity of DiSC3(5) are shown in Fig. 6I and J; that is, the fluorescence intensity significantly increased when the TS-CATH concentration was above 4 μg/ml, and the highest fluorescence intensity was equivalent to that of the positive control melittin, indicating that TS-CATH can dissipate the membrane potential by permeating the membrane.

3.7. TS-CATH induced dysfunction of the bacterial respiratory chain

The chemiosmotic theory suggests that protons pumped by the respiratory chain are driven by the proton dynamic potential back into the cytosol by ATP synthase, where they are coupled to generate ATP. CCCP is an oxidative phosphorylation uncoupling agent that reduces protons back to the cytosol via ATP synthase. The changes in the bacterial ATP concentration after coincubation with bacteria at sub-MICs (<4 μg/ml) of TS-CATH were determined to explore whether the depolarization of the membrane potential by TS-CATH affects the accumulation of bacterial ATP. The results showed that the peptide TS-CATH decreased ATP accumulation in a dose-dependent manner in *P. aeruginosa* (Fig. 7B), and when TS-CATH reached 4 μg/ml, the ATP level was comparable to that of the uncoupled positive control CCCP. In *E. coli* E24, 1 μg/ml (1/4 ×MIC) TS-CATH significantly inhibited total ATP accumulation by 50% (Fig. 7A).

To further explore the effects of TS-CATH on the bacterial respiratory chain, the NADH levels were subsequently measured by resazurin [53]. Resazurin can be reduced by NADH to the red fluorescent dye resorufin in cells, and the fluorescence intensity of resorufin reflects the content of NADH. For *E. coli* E24 (Fig. 7C), TS-CATH at sub-MICs promoted the production of resorufin in a dose-dependent manner, suggesting the loss of NADH. However, a higher concentration of TS-CATH promoted NADH amassing at the initial stage, which slowed in 150 min. Similar phenomena were found for *P. aeruginosa* (Fig. 7D). TS-CATH enhanced the production of resorufin in a dose-dependent manner, but there was no significant difference in NADH accumulation after treatment with TS-CATH above the MIC. The content of NADH not only decreased but

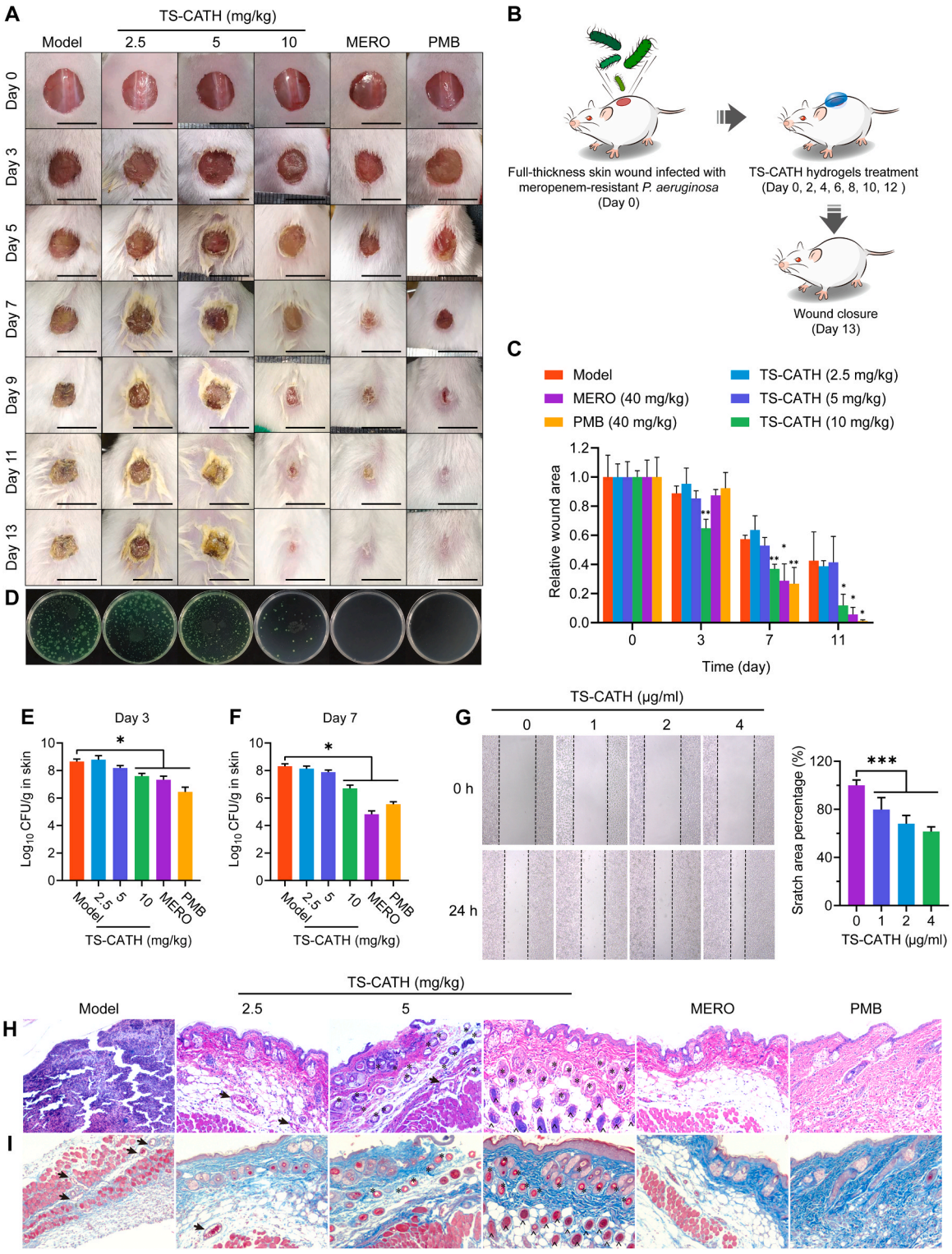

Fig. 5. TS-CATH protected mice against drug-resistant *P. aeruginosa*-induced wound infection. (A) Representative images of the wound healing process of mice treated with TS-CATH hydrogel (2.5, 5, and 10 mg/kg), black hydrogel, meropenem solution (MERO, 40 mg/kg), or compound polymyxin B ointment (PMB, 40 mg/kg). Scale bar, 1 μm. (B) Schematic diagram illustrating the timeline of the experimental process. (C) Quantitative analysis of the relative wound areas at different time points. (D) Photographs of agar plates of skin wound tissues on day 7. (E–F) Bacterial counts in mouse skin wound tissues at days 3 and 7. (G) Cell scratch assay for cell migration (left) and quantification (right). (H) H&E (×100) and (I) Masson staining images (×100) of skin wound tissues on day 7. Black arrows: enlarged blood vessels; "* ": sweat glands; "^": hair follicles. The data are presented as the means ± SDs. Statistical analyses were performed using a two-tailed Student's t test (C) or one-way ANOVA (E–G). * $P < 0.05$, * * $P < 0.01$, * ** $P < 0.001$, and ns, not significant, compared with the model. The data are presented as the means ± SDs.

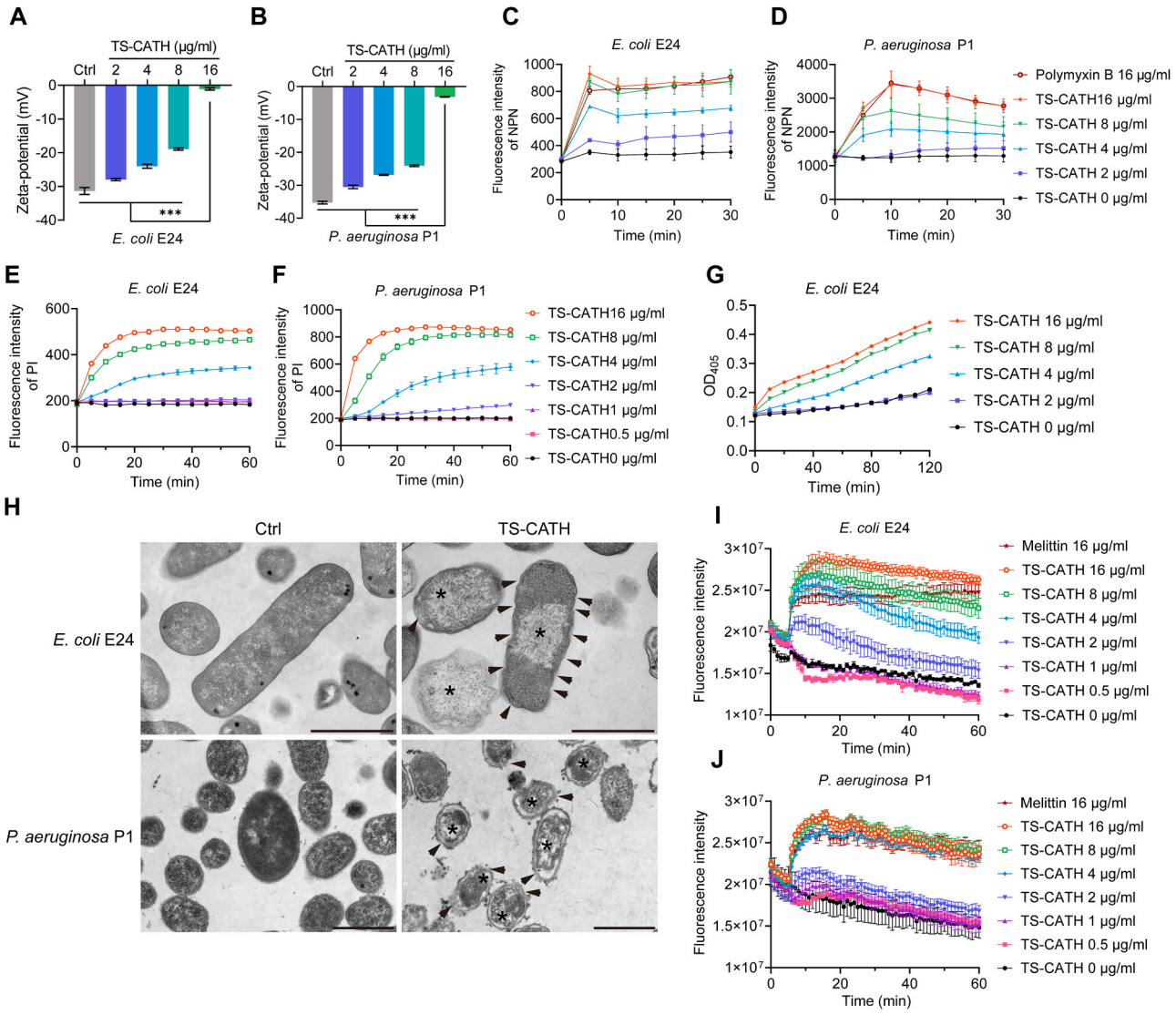

Fig. 6. TS-CATH induced destabilization of the bacterial membrane. (A–B) Zeta potential detection of *E. coli* E24 and *P. aeruginosa* P1 treated with TS-CATH. (C–D) The outer membrane permeability of TS-CATH determined by detecting NPN fluorescence. Polymyxin B at 16 μg/ml was used as a positive control. (E–F) TS-CATH dosage-related membrane permeability was measured by the increased fluorescence of PI. (G) TS-CATH dose-related leakage of intracellular contents was detected by the release of cytoplasmic β-galactosidase from *E. coli* E24, which hydrolyzed ONPG to yellow 2-nitrophenol at an absorbance of 420 nm. (H) TEM images of TS-CATH-induced *E. coli* E24 and *P. aeruginosa* P1 membrane disruption and leakage of the cytoplasmic contents. Arrows: damaged membrane; "* ": leakage of cytoplasmic contents. Scale bar, 1 μm. (I–J) The dissipation of bacterial membrane potential was determined by the increase in DiSC3(5) fluorescence for several TS-CATH dosage treatments. Statistical analyses were performed using two-tailed one-way ANOVA. * $P < 0.05$, * * $P < 0.01$, * ** $P < 0.001$, and ns, not significant. The data are presented as the means ± SDs.

also increased with the addition of TS-CATH, suggesting that TS-CATH may inhibit the activity of NADH dehydrogenase in the respiratory chain, resulting in the accumulation of NADH dehydrogenase substrates. Moreover, exogenously added TTC, a membrane-permeable substrate of respiratory chain dehydrogenase, can be oxidized to the red formazan compound triphenylformazan (TF) by dehydrogenase. The absorbance of red TF was measured to explore the change in dehydrogenase activity. As illustrated in Fig. 7E and F, coincubation of TS-CATH with bacteria for 1 h reduced dehydrogenase activity in a dose-dependent manner, which was halved at a sub-MIC of 2 μg/ml. Furthermore, the expression levels of the respiratory chain dehydrogenase genes *ndh* and *sdhC* in *E. coli* E24 were inhibited in a time-dependent manner in response to treatment with TS-CATH at sub-MICs (Fig. 7G and H). The gel retardation results revealed that TS-CATH bound to *E. coli* E24 genomic DNA and *P. aeruginosa* P1 genomic DNA (Fig. 7K and L), which may interfere with synthesis, replication, and translational processes [60,61]. The data above suggest that TS-CATH suppresses the activity of NADH dehydrogenase and succinate dehydrogenase by inhibiting their gene expression.

3.8. TS-CATH promoted antimicrobial effects by inducing ROS

Disruption of the respiratory chain is accompanied by ROS formation. The ROS probe DCFH-DA can be hydrolyzed by esterase, retained in the cell and subsequently oxidized by intracellular ROS to produce the fluorescent substance DCF. The fluorescence intensity of DCF reflects the level of intracellular ROS. TS-CATH promoted the production of ROS in bacteria in a dose-dependent manner, and the level of ROS induced was comparable to that of the positive control polymyxin B (Fig. 7M). Moreover, the ROS production induced by TS-CATH could be suppressed by the addition of the ROS scavenger NAC, the Fenton reaction inhibitor dipyridine (DP), and the hydroxyl radical scavenger thiourea (TU), suggesting the induction of hydroxyl radical formation (Fig. 7N). In addition, the superoxide dismutase gene *SodB* was significantly

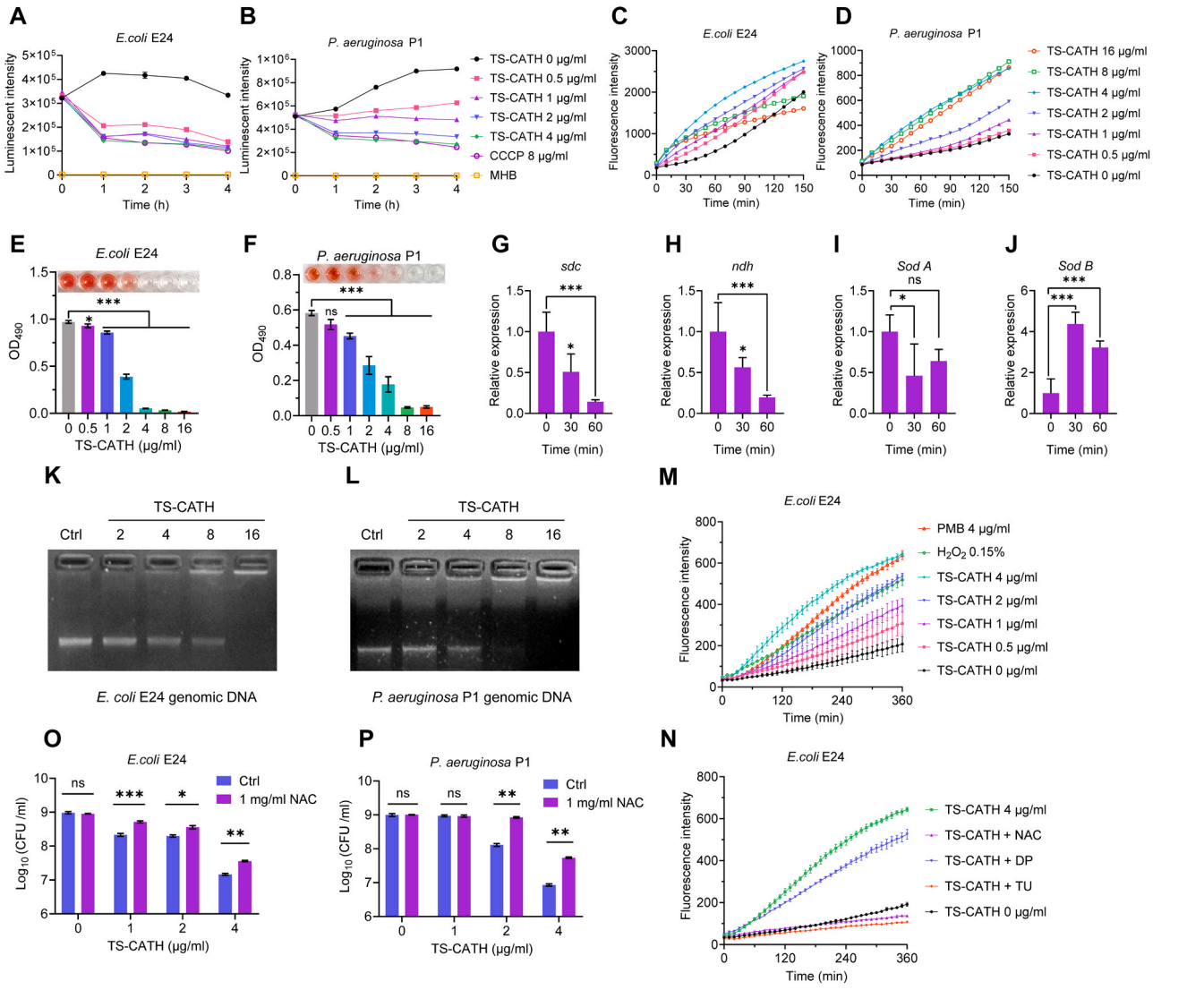

Fig. 7. TS-CATH induced disruption of the bacterial respiratory chain and the accumulation of ROS. (A–B) Intracellular ATP levels at different TS-CATH concentrations. Treatment with 40 μg/ml CCCP was used as a positive control. (C–D) Reduction of resazurin to resorufin by NADH at different TS-CATH concentrations. (E–F) Respiratory chain dehydrogenase activity inhibition was detected by the oxidation of colorless TTC to triphenylformazan (TF) at an absorbance of 480 nm. (G–H) The expression levels of dehydrogenase genes (*ndh* and *sdhC*) and (I–J) superoxide dismutase genes (*sodA* and *sodB*) in *E. coli* E24 in response to treatment with TS-CATH at sub-MIC (2 μg/ml). (K–L) DNA binding activity of TS-CATH to genomic DNA. (M) Total ROS accumulation in *E. coli* E24 treated with TS-CATH was recorded by the probe DCFH-DA·H_2O_2 (0.15%) and polymyxin B (4 μg/ml) were used as positive controls. (N) Exogenous addition of the ROS scavenger NAC or the ROS inhibitors DP and TU diminished the TS-CATH-induced accumulation of ROS. (O–P) Colony-forming units of *E. coli* at increasing dosages of TS-CATH in the presence or absence of NAC. Statistical analyses were performed using a two-tailed Student's t test or one-way ANOVA. * $P < 0.05$, * * $P < 0.01$, * ** $P < 0.001$, and ns, not significant. The data are presented as the means ± SDs.

increased after sub-MIC (2 μg/ml) TS-CATH treatment, further indicating that TS-CATH induced intracellular ROS production, while the expression level of *SodA* was slightly reduced (Fig. 7I and J).

Due to the strong oxidative activity of hydroxyl radicals and the extreme destruction of proteins and DNA, TS-CATH could exert its antimicrobial effect by inducing ROS. The effect of induced ROS on bacterial growth was explored by adding an ROS scavenger during the coincubation of TS-CATH with bacteria. The inclusion of NAC did not alter the growth rate of normal bacteria; nonetheless, after coincubation with sub-MIC of TS-CATH, the number of bacterial CFUs was significantly greater than that observed following treatment with TS-CATH alone (Fig. 7O and P). The addition of NAC partially restrained the antibacterial activity of TS-CATH, which also confirmed that TS-CATH could exert its antimicrobial effect by inducing ROS. Taken together, the results showed that TS-CATH destabilized the bacterial membrane and disrupted the bacterial respiratory chain, leading to the generation of additional ROS and ultimately undermining bacterial growth (Fig. 8).

3.9. Activity stability in salt and serum

Infection-associated skin edema is marked by the accumulation of fluid, leading to swelling and subsequent creation of a microenvironment with a high salt concentration. As a result, peptides must maintain their activity in environments containing high salt concentrations [62,63]. As shown in Table S5, TS-CATH maintained antimicrobial activity as the salt concentration increased from 100 to 150 mmol. Many conventional antibiotics, such as β-lactams, cephalosporins, tetracyclines, and quinolones, are unstable in aqueous solutions [64]. In addition, TS-CATH retained its bactericidal activity after being incubated at a wide range of temperatures (37–90 °C) (Table S6). Issues have been raised regarding the stability of peptidic drugs for systemic use, and their serum stability was further investigated. After incubation with

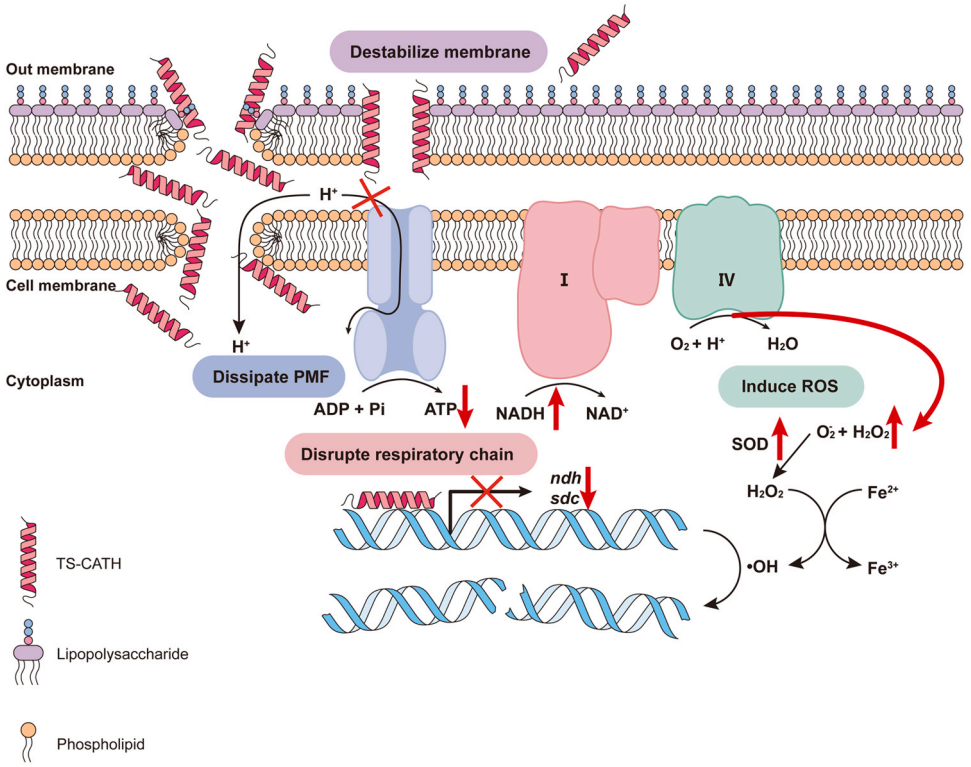

Fig. 8. Proposed antimicrobial mechanism of TS-CATH. TS-CATH destabilized the bacterial membrane and disrupted the bacterial respiratory chain, leading to the generation of additional ROS and ultimately undermining bacterial growth.

25% fresh mouse serum for up to 2 h, TS-CATH retained antimicrobial activity but with a 4-fold increase in MIC (Table S7). This increase may be attributed to protease degradation in the serum [65,66]. Overall, TS-CATH, which has systemic or local applications, is resistant to NaCl, temperature, and serum.

4. Discussion

In 2019, bacterial antimicrobial resistance was responsible for approximately 1.2 million deaths globally [67]. Antimicrobial peptides are promising therapeutic agents for treating drug-resistant bacterial disease, which is attributed to decreased susceptibility to evolutionary resistance. In this study, novel cathelicidin protein precursors were obtained from *Thamnophis sirtalis*, *Balaenoptera musculus,* and *Lipotes vexillifer*. After confirming the conserved sequence, the mature peptide sequences were truncated and named TS-CATH, BM-CATH, and LV-CATH.

These three peptides have a high α-helix contents in a hydrophobic environment with high hydrophobicity, hydrophobic moments, and positive charges. α-Helical peptides are often unstructured in aqueous solution but adopt an amphipathic helical structure when in contact with a biological membrane [68]. These three peptides exhibited broad-spectrum antimicrobial activity against gram-negative bacteria, including *E. coli*, *P. aeruginosa*, *K. pneumoniae,* and *A. baumannii*, while TS-CATH had little effect on *S. aureus*. Due to the excellent antimicrobial activity and negligible cytotoxicity of TS-CATH, it was selected for continued bactericidal effect assessment *in vitro* and *in vivo*.

TS-CATH has been shown to have effective and rapid bactericidal activity against drug-resistant clinically isolated pathogens, with MBCs within 4 ×MICs, and completely killed gram-negative bacteria at 4 ×MIC in 20 min. Other peptides, such as magainin 2 [69], cecropin P1 [70], PR-39 [70], and SMAP29 [71], have been shown to kill bacteria in 15–90 min. AMPs demonstrate more rapid bactericidal activity than small-molecule antibiotics, achieving this effect within minutes rather than hours [21]. This faster bactericidal effect results in reduced evolutionary pressure, as bacteria have fewer opportunities for the generation and development of resistance. Compared with normal mammalian cells, TS-CATH also maintained a satisfactory killing effect on pathogens at the MBC. This selectivity arises from fundamental differences in surface charge and composition between host cells and pathogenic bacteria [72,73]. Furthermore, the leucine/isoleucine zipper structures present in BM-CATH and LV-CATH but absent in TS-CATH, where every seventh amino acid residue is either leucine or isoleucine, play critical roles in mediating their cytotoxicity to mammalian cells. However, the same motif does not contribute substantially to the antibacterial activity of these compounds [74,75], which may help explain the inferior selective cytotoxicity of BM-CATH and LV-CATH.

E. coli is the most common causative agent of infections acquired in hospital and community settings [76]. A bacteremia model involving the injection of ceftazidime-resistant *E. coli* was constructed to explore the protective effect of the peptide on acute infection. Under lethal infection with *E. coli*, TS-CATH dose-dependently improved the survival rate to 85.7% in mice, possibly because of its potent bactericidal effects. Moreover, TS-CATH may inhibit the bacterium-induced inflammatory response because it was reported that nonhuman cathelicidins can suppress the LPS-induced inflammatory response by suppressing TLR4 signaling [77].

P. aeruginosa causes serious infection and septic mortality in burn patients, particularly when it is nosocomially acquired [78]. A high dose of the TS-CATH hydrogel promoted wound healing and accelerated the wound healing rate by significantly reducing the bacterial load in the wound tissue. However, TS-CATH at dosages of 2.5 or 5 mg/kg had little effect on wound healing, which may be attributed to the deficiency of the dosage compared with those of the positive control drugs. Similarly, LL-37 can also promote angiogenesis, wound healing [27,79], and re-epithelialization of wounds [28]. These phenotypic changes are attributed to the activation of signaling intermediates and transcription factors mediated by the peptide [27]. Whether TS-CATH accelerates

wound healing through these mechanisms needs further exploration.

Due to their special amphiphilic structural characteristics, antimicrobial peptides can directly damage the cell walls and membranes of bacteria but cannot easily cause drug resistance. In addition, a variety of mechanisms involving intracellular antimicrobial peptide targets, such as binding to virulence proteins to inhibit the activity of virulence proteins and inhibiting the biosynthesis of DNA, RNA, or proteins, have been widely reported [16,42,45]. In this study, the bacterial surface potential was significantly neutralized after TS-CATH treatment, revealing that TS-CATH could interact with bacteria via electrostatic interactions. Teichoic acids are present in the cell walls of gram-positive bacteria, and lipopolysaccharides (LPS) in the outer membranes of gram-negative bacteria contribute to the electronegative charge of the bacterial surface. This charging profile is highly attractive for positively charged AMPs [73]. Subsequently, a series of assays, including NPN, PI staining, ONPG, and TEM assays, all showed that TS-CATH can damage the bacterial outer and inner cell membranes, leading to the leakage of bacterial internal proteins. There was a difference in the base values of the NPN uptake assay between *E. coli* and *P. aeruginosa*, resulting in different increasing fluorescence intensities of NPN, as shown in Fig. 6C and D; this difference may be ascribed to the different membrane compositions of *E. coli* and *P. aeruginosa* leading to differences in hydrophobicity [80,81]. The membrane potential plays a crucial role in maintaining the functions of membrane proteins, such as those used for voltage-gated ionic channels and the synthesis of ATP [82]. Indeed, TS-CATH depolarized the difference in the membrane potential between the two sides of the cell membrane in a dose-dependent manner.

Because TS-CATH can destroy the bacterial cell membrane where the respiratory chain is located, the disruption effect of the respiratory chain was further explored. The respiratory chain pumps protons to the outside of the membrane via transmembrane proteins, resulting in an electrochemical gradient between the separate sides of the cell membrane. TS-CATH inhibited ATP accumulation in a dose-dependent manner at sub-MICs, suggesting that TS-CATH could disrupt the bacterial inner membrane and promote the efflux of protons from the membrane, possibly by acting as a respiratory chain uncoupling agent. Proton-pumping NADH:ubiquinone oxidoreductase, also called complex I, is the first respiratory complex to provide the proton motive force by proton-coupled electron transfer reactions from NADH to oxygen, which is essential for ATP synthesis [83]. Thus, the activity of NADH dehydrogenase was further investigated. TS-CATH at sub-MICs upregulated NADH levels and promoted NADH accumulation, indicating that TS-CATH can inhibit the activity of NADH dehydrogenase in the respiratory chain. Although resazurin was used to determine cell viability [84], it was also used to monitor the NADH level to characterize the activity of NADH dehydrogenase [53,85,86]. The gene expression levels of NADH dehydrogenase and succinate dehydrogenase decreased after *E. coli* were treated with sub-MIC of TS-CATH, suggesting that the inhibition of NADH dehydrogenase gene expression and activity promotes the accumulation of NADH and ATP. Notably, earlier research revealed that polymyxin B treatment could also decrease the level of NADH dehydrogenase and induce aberrant oxidative respiration [87,88].

Excessive ROS produced when the respiratory chain is disrupted can further damage biological macromolecules in bacteria while inducing antioxidant enzymes to eradicate ROS [53,89]. In a dose-dependent manner, TS-CATH induced the production of ROS, including hydroxyl radicals, which could be suppressed by the addition of the hydroxyl radical scavenger TU and the Fenton reaction inhibitor DP. Disruptions in the electron transport chain can promote the production of superoxide, which can participate in the Fenton reaction, leading to the generation of hydroxyl radicals [90–92]. SodA and SodB are superoxide dismutases that defend against oxidative stress through the decomposition of superoxide radicals in *E. coli*. SodA is more effective at preventing damage to DNA, while SodB is more effective at protecting against cytoplasmic superoxide-sensitive enzymes [93]. While SodA and SodB synthesis are completely opposed in *E. coli* [94], TS-CATH induced significant upregulation of the *SodB* gene and slight downregulation of the *SodA* gene, revealing that oxidative stress occurred in these cells. This oxidative stress could cause structural damage to cellular macromolecules such as DNA, lipids, and proteins and ultimately cause bacterial death [90,91,95]. Polymyxin treatment has been shown to induce hydroxyl radical production through the Fenton reaction, which mediates the rapid killing of *A. baumannii* and *E. coli* [95]. The ROS scavenger NAC significantly inhibited the antibacterial activity of TS-CATH, suggesting that ROS induction was involved in the inhibitory effect of TS-CATH on bacterial growth. In earlier studies, cathelicidin peptides were found to induce ROS production in bacteria, leading to bacterial growth restriction through perturbation of bacterial membranes ROS induction [89,92,96].

In summary, this study demonstrated that TS-CATH from *Thamnophis sirtalis* has rapid and potent broad-spectrum bactericidal activity against drug-resistant pathogens *in vitro*. Moreover, TS-CATH effectively rescued mice with bacteremia and ameliorated infected wounds by directly killing bacteria through the destabilization and rupture of their membranes. At sub-MICs, TS-CATH disrupted the bacterial respiratory chain, leading to the inhibition of ATP accumulation and the induction of additional ROS, ultimately undermining bacterial growth. Therefore, these findings highlight TS-CATH as a promising therapeutic agent for treating drug-resistant bacterial infections.

CRediT authorship contribution statement

Changlin Zhou: Funding acquisition. **Xiaolin Xie:** Visualization. **Lingman Ma:** Funding acquisition, Project administration, Supervision, Validation, Writing – review & editing. **Meina Zhang:** Formal analysis, Software, Visualization, Writing – review & editing. **Jian Wang:** Conceptualization, Data curation, Methodology, Validation, Visualization, Writing – original draft, Writing – review & editing. **Mengyuan Liu:** Methodology, Visualization. **Chao Li:** Data curation, Validation, Visualization. **Yixin Qi:** Methodology, Visualization.

Declaration of Competing Interest

The authors declare that they have no known competing financial interests or personal relationships that could have appeared to influence the work reported in this paper.

Acknowledgments

This work was funded by the National Key Research and Development Program of China (2018YFA0902000), the National Natural Science Foundation of China (No. 82173863), the Double First-Class University project (CPU2022QZ09), the Natural Science Foundation of Jiangsu Province of China (No. BK20201327), and the Priority Academic Program Development of Jiangsu Higher Education Institutions. We thank Jiangsu Women and Children Health Hospital (Nanjing, Jiangsu, China) for kindly providing the clinical isolate strains and Wei Liu for helping with the language.

Declaration of Competing Interests

All the authors declare that no competing interests exist.

Appendix A. Supporting information

Supplementary data associated with this article can be found in the online version at doi:10.1016/j.csbj.2024.05.020.

References

[1] Brown ED, Wright GD. Antibacterial drug discovery in the resistance era. Nature 2016;529(7586):336–43. Epub 2016/01/23. doi: 10.1038/nature17042. PubMed PMID: 26791724.

[2] McEwen SA, Collignon PJ. Antimicrobial resistance: a one health perspective. Microbiol Spectr 2018;6(2). Epub 2018/03/31. doi: 10.1128/microbiolspec.ARBA-0009-2017. PubMed PMID: 29600770.

[3] Darby EM, Trampari E, Siasat P, Gaya MS, Alav I, Webber MA, et al. Molecular mechanisms of antibiotic resistance revisited. Nat Rev Microbiol 2022. Epub 2022/11/22. doi: 10.1038/s41579-022-00820-y. PubMed PMID: 36411397.

[4] Jiang Q, Feng M, Ye C, Yu X. Effects and relevant mechanisms of non-antibiotic factors on the horizontal transfer of antibiotic resistance genes in water environments: a review. Sci Total Environ 2022;806(Pt 3)):150568. Epub 2021/10/10. doi: 10.1016/j.scitotenv.2021.150568. PubMed PMID: 34627113.

[5] MacNair CR, Tan MW. The role of bacterial membrane vesicles in antibiotic resistance. Ann N Y Acad Sci 2023;1519(1):63–73. Epub 2022/11/23. doi: 10.1111/nyas.14932. PubMed PMID: 36415037.

[6] Davies J, Davies D. Origins and evolution of antibiotic resistance. Microbiol Mol Biol Rev 2010;74(3):417–33. Epub 2010/09/02. doi: 10.1128/mmbr.00016-10. PubMed PMID: 20805405; PubMed Central PMCID: PMCPMC2937522.

[7] Tsiodras S, Gold HS, Sakoulas G, Eliopoulos GM, Wennersten C, Venkataraman L, et al. Linezolid resistance in a clinical isolate of Staphylococcus aureus. Lancet (Lond, Engl) 2001;358(9277):207–8. Epub 2001/07/31. doi: 10.1016/s0140-6736(01)05410-1. PubMed PMID: 11476839.

[8] Stefani S, Campanile F, Santagati M, Mezzatesta ML, Cafiso V, Pacini G. Insights and clinical perspectives of daptomycin resistance in Staphylococcus aureus: a review of the available evidence. Int J Antimicrob Agents 2015;46(3):278–89. Epub 2015/07/06. doi: 10.1016/j.ijantimicag.2015.05.008. PubMed PMID: 26143590.

[9] Mangili A, Bica I, Snydman DR, Hamer DH. Daptomycin-resistant, methicillin-resistant Staphylococcus aureus bacteremia. Clin Infect Dis: Publ Infect Dis Soc Am 2005;40(7):1058–60. Epub 2005/04/13. doi: 10.1086/428616. PubMed PMID: 15825002.

[10] Kaye KS, Pogue JM, Tran TB, Nation RL, Li J. Agents of last resort: polymyxin resistance. Infect Dis Clin North Am 2016;30(2):391–414. Epub 2016/05/22. doi: 10.1016/j.idc.2016.02.005. PubMed PMID: 27208765.

[11] Sun J, Zhang H, Liu YH, Feng Y. Towards understanding MCR-like colistin resistance. Trends Microbiol 2018;26(9):794–808. Epub 2018/03/12. doi: 10.1016/j.tim.2018.02.006. PubMed PMID: 29525421.

[12] Yang Q, Li M, Spiller OB, Andrey DO, Hinchliffe P, Li H, et al. Balancing mcr-1 expression and bacterial survival is a delicate equilibrium between essential cellular defence mechanisms. Nat Commun 2017;8(1):2054. Epub 2017/12/14. doi: 10.1038/s41467-017-02149-0. PubMed PMID: 29233990; PubMed Central PMCID: PMCPMC5727292.

[13] Jenssen H, Hamill P, Hancock RE. Peptide antimicrobial agents. Clin Microbiol Rev 2006;19(3):491–511. Epub 2006/07/19. doi: 10.1128/cmr.00056-05. PubMed PMID: 16847082; PubMed Central PMCID: PMCPMC1539102.

[14] Hancock REW, Alford MA, Haney EF. Antibiofilm activity of host defence peptides: complexity provides opportunities. Nat Rev Microbiol 2021;19(12):786–97. Epub 2021/06/30. doi: 10.1038/s41579-021-00585-w. PubMed PMID: 34183822.

[15] Mahlapuu M, Håkansson J, Ringstad L, Björn C. Antimicrobial peptides: an emerging category of therapeutic agents. Front Cell Infect Microbiol 2016;6. 194. Epub 2017/01/14. doi: 10.3389/fcimb.2016.00194. PubMed PMID: 28083516; PubMed Central PMCID: PMCPMC5186781.

[16] Mookherjee N, Anderson MA, Haagsman HP, Davidson DJ. Antimicrobial host defence peptides: functions and clinical potential. Nat Rev Drug Discov 2020;19(5):311–32. Epub 2020/02/29. doi: 10.1038/s41573-019-0058-8. PubMed PMID: 32107480.

[17] Brogden KA. Antimicrobial peptides: pore formers or metabolic inhibitors in bacteria? Nat Rev Microbiol 2005;3(3):238–50. Epub 2005/02/11. doi: 10.1038/nrmicro1098. PubMed PMID: 15703760.

[18] Hancock RE, Sahl HG. Antimicrobial and host-defense peptides as new anti-infective therapeutic strategies. Nat Biotechnol 2006;24(12):1551–7. Epub 2006/12/13. doi: 10.1038/nbt1267. PubMed PMID: 17160061.

[19] Yu G, Baeder DY, Regoes RR, Rolff J. Predicting drug resistance evolution: insights from antimicrobial peptides and antibiotics. Proc Biol Sci 2018;285(1874). Epub 2018/03/16. doi: 10.1098/rspb.2017.2687. PubMed PMID: 29540517; PubMed Central PMCID: PMCPMC5879628.

[20] Spohn R, Daruka L, Lázár V, Martins A, Vidovics F, Grézal G, et al. Integrated evolutionary analysis reveals antimicrobial peptides with limited resistance. Nat Commun 2019;10(1):4538. Epub 2019/10/06. doi: 10.1038/s41467-019-12364-6. PubMed PMID: 31586049; PubMed Central PMCID: PMCPMC6778101.

[21] Lazzaro BP, Zasloff M, Rolff J. Antimicrobial peptides: application informed by evolution. Sci (N Y, NY) 2020;368(6490). Epub 2020/05/02. doi: 10.1126/science.aau5480. PubMed PMID: 32355003; PubMed Central PMCID: PMCPMC8097767.

[22] Alford MA, Baquir B, Santana FL, Haney EF, Hancock REW. Cathelicidin host defense peptides and inflammatory signaling: striking a balance. Front Microbiol 2020;11:1902. Epub 2020/09/29. doi: 10.3389/fmicb.2020.01902. PubMed PMID: 32982998; PubMed Central PMCID: PMCPMC7481365.

[23] Zasloff M. Antimicrobial peptides in health and disease. N Engl J Med 2002;347(15):1199–200. Epub 2002/10/11. doi: 10.1056/NEJMe020106. PubMed PMID: 12374882.

[24] Scott MG, Davidson DJ, Gold MR, Bowdish D, Hancock RE. The human antimicrobial peptide LL-37 is a multifunctional modulator of innate immune responses. J Immunol (Baltim, Md: 1950) 2002;169(7):3883–91. Epub 2002/09/24. doi: 10.4049/jimmunol.169.7.3883. PubMed PMID: 12244186.

[25] De Y, Chen Q, Schmidt AP, Anderson GM, Wang JM, Wooters J, et al. LL-37, the neutrophil granule- and epithelial cell-derived cathelicidin, utilizes formyl peptide receptor-like 1 (FPRL1) as a receptor to chemoattract human peripheral blood neutrophils, monocytes, and T cells. J Exp Med 2000;192(7):1069–74. Epub 2000/10/04. doi: 10.1084/jem.192.7.1069. PubMed PMID: 11015447; PubMed Central PMCID: PMCPMC2193321.

[26] Barlow PG, Beaumont PE, Cosseau C, Mackellar A, Wilkinson TS, Hancock RE, et al. The human cathelicidin LL-37 preferentially promotes apoptosis of infected airway epithelium. Am J Respir Cell Mol Biol 2010;43(6):692–702. Epub 2010/01/26. doi: 10.1165/rcmb.2009-0250OC. PubMed PMID: 20097832; PubMed Central PMCID: PMCPMC2993089.

[27] Carretero M, Escámez MJ, García M, Duarte B, Holguín A, Retamosa L, et al. In vitro and in vivo wound healing-promoting activities of human cathelicidin LL-37. J Invest Dermatol 2008;128(1):223–36. Epub 2007/09/07. doi: 10.1038/sj.jid.5701043. PubMed PMID: 17805349.

[28] Heilborn JD, Nilsson MF, Kratz G, Weber G, Sørensen O, Borregaard N, et al. The cathelicidin anti-microbial peptide LL-37 is involved in re-epithelialization of human skin wounds and is lacking in chronic ulcer epithelium. J Investig Dermatol 2003;120(3):379–89. Epub 2003/02/27. doi: 10.1046/j.1523-1747.2003.12069.x. PubMed PMID: 12603850.

[29] Lehrer RI, Ganz T. Cathelicidins: a family of endogenous antimicrobial peptides. Curr Opin Hematol 2002;9(1):18–22. Epub 2001/12/26. doi: 10.1097/00062752-200201000-00004. PubMed PMID: 11753073.

[30] Kościuczuk EM, Lisowski P, Jarczak J, Strzałkowska N, Jóźwik A, Horbańczuk J, et al. Cathelicidins: family of antimicrobial peptides. A review. Mol Biol Rep 2012;39(12):10957–70. Epub 2012/10/16. doi: 10.1007/s11033-012-1997-x. PubMed PMID: 23065264; PubMed Central PMCID: PMCPMC3487008.

[31] Wassing GM, Bergman P, Lindbom L, van der Does AM. Complexity of antimicrobial peptide regulation during pathogen-host interactions. Int J Antimicrob Agents 2015;45(5):447–54. Epub 2014/12/24. doi: 10.1016/j.ijantimicag.2014.11.003. PubMed PMID: 25532742.

[32] Bals R, Wilson JM. Cathelicidins–a family of multifunctional antimicrobial peptides. Cell Mol life Sci: CMLS 2003;60(4):711–20. Epub 2003/06/06. doi: 10.1007/s00018-003-2186-9. PubMed PMID: 12785718.

[33] Cai S, Qiao X, Feng L, Shi N, Wang H, Yang H, et al. Python cathelicidin CATHPb1 protects against multidrug-resistant staphylococcal infections by antimicrobial-immunomodulatory duality. J Med Chem 2018;61(5):2075–86. Epub 2018/02/22. doi: 10.1021/acs.jmedchem.8b00036. PubMed PMID: 29466000.

[34] Zhang L, Jie H, Xiao Y, Zhou C, Lyu W, Bai W. Genomic identification and expression analysis of the cathelicidin gene family of the forest musk deer. Anim: Open Access J Mdpi 2019;9(8). Epub 2019/07/28. doi: 10.3390/ani9080481. PubMed PMID: 31344924; PubMed Central PMCID: PMCPMC6719980.

[35] Zhong L, Liu J, Teng S, Xie Z. Identification of a Novel Cathelicidin from the Deinagkistrodon acutus Genome with Antibacterial Activity by Multiple Mechanisms. Toxins 2020;12(12). Epub 2020/12/10. doi: 10.3390/toxins12120771. PubMed PMID: 33291852; PubMed Central PMCID: PMCPMC7762006.

[36] Barksdale SM, Hrifko EJ, van Hoek ML. Cathelicidin antimicrobial peptide from Alligator mississippiensis has antibacterial activity against multi-drug resistant Acinetobacter baumanii and Klebsiella pneumoniae. Dev Comp Immunol 2017;70:135–44. Epub 2017/01/17. doi: 10.1016/j.dci.2017.01.011. PubMed PMID: 28089718.

[37] Keil B. Specificity of proteolysis. Springer Berlin Heidelberg; 1992.

[38] Barrett AJ. Handbook of proteolytic enzymes. Elsevier; 2004.

[39] CLSI. Methods for Dilution Antimicrobial Susceptibility Tests for Bacteria That Grow Aerobically. Clinical and Laboratory Standards Institute. 2018;12th ed. CLSI standard M07.

[40] Jiang M, Ma L, Huang Y, Wu H, Dou J, Zhou C. Antimicrobial activities of peptide Cbf-K(16) against drug-resistant Helicobacter pylori infection in vitro and in vivo. Microb Pathog 2020;138:103847. Epub 2019/11/11. doi: 10.1016/j.micpath.2019.103847. PubMed PMID: 31704464.

[41] Khara JS, Lim FK, Wang Y, Ke XY, Voo ZX, Yang YY, et al. Designing α-helical peptides with enhanced synergism and selectivity against Mycobacterium smegmatis: discerning the role of hydrophobicity and helicity. Acta Biomater 2015;28:99–108. Epub 2015/09/19. doi: 10.1016/j.actbio.2015.09.015. PubMed PMID: 26380930.

[42] Ma L, Xie X, Liu H, Huang Y, Wu H, Jiang M, et al. Potent antibacterial activity of MSI-1 derived from the magainin 2 peptide against drug-resistant bacteria. Theranostics 2020;10(3):1373–90. Epub 2020/01/16. doi: 10.7150/thno.39157. PubMed PMID: 31938070; PubMed Central PMCID: PMCPMC6956804.

[43] Friedrich C, Scott MG, Karunaratne N, Yan H, Hancock RE. Salt-resistant alpha-helical cationic antimicrobial peptides. Antimicrob Agents Chemother 1999;43(7):1542–8. Epub 1999/07/02. doi: 10.1128/aac.43.7.1542. PubMed PMID: 10390200; PubMed Central PMCID: PMCPMC89321.

[44] Zhu Y, Shao C, Li G, Lai Z, Tan P, Jian Q, et al. Rational avoidance of protease cleavage sites and symmetrical end-tagging significantly enhances the stability and therapeutic potential of antimicrobial peptides. J Med Chem 2020;63(17):9421–35. Epub 2020/07/25. doi: 10.1021/acs.jmedchem.0c00583. PubMed PMID: 32706256.

[45] Jiang M, Yang X, Wu H, Huang Y, Dou J, Zhou C, et al. An active domain HF-18 derived from hagfish intestinal peptide effectively inhibited drug-resistant bacteria in vitro/vivo. Biochem Pharmacol 2020;172:113746. Epub 2019/12/10. doi: 10.1016/j.bcp.2019.113746. PubMed PMID: 31812678.

[46] Kumbhar S, Khairate R, Bhatia M, Choudhari P, Gaikwad V. Evaluation of curcumin-loaded chitosan nanoparticles for wound healing activity. Admet dmpk 2023;11(4):601–13. Epub 2023/11/08. doi: 10.5599/admet.1897. PubMed PMID: 37937244; PubMed Central PMCID: PMCPMC10626514.
[47] Imad R, Sheikh Z, Rao Pichika M, Kit-Kay M, Siddiqui RA, Nawaid Shah SN, et al. Cathepsin-K inhibition enhances anti-cancerous activity within oral squamous cell carcinoma cells: uncloaking the potency of new K21 formulation. Exp Cell Res 2023;430(1):113687. Epub 2023/06/26. doi: 10.1016/j.yexcr.2023.113687. PubMed PMID: 37356748.
[48] Lai Z, Jian Q, Li G, Shao C, Zhu Y, Yuan X, et al. Self-assembling peptide dendron nanoparticles with high stability and a multimodal antimicrobial mechanism of action. ACS Nano 2021;15(10):15824–40. Epub 2021/09/23. doi: 10.1021/acsnano.1c03301. PubMed PMID: 34549935.
[49] Dumpati S, Dutta D. Bacterial dye release measures in response to antimicrobial peptides. Methods Mol Biol (Clifton, NJ) 2022;2402:285–90. Epub 2021/12/03. doi: 10.1007/978-1-0716-1843-1_21. PubMed PMID: 34854051.
[50] Lesnichaya M, Perfileva A, Nozhkina O, Gazizova A, Graskova I. Synthesis, toxicity evaluation and determination of possible mechanisms of antimicrobial effect of arabinogalactane-capped selenium nanoparticles. J Trace Elem Med Biol: Organ Soc Miner Trace Elem (GMS) 2022;69:126904. Epub 2021/11/26. doi: 10.1016/j.jtemb.2021.126904. PubMed PMID: 34823103.
[51] Tachon S, Michelon D, Chambellon E, Cantonnet M, Mezange C, Henno L, et al. Experimental conditions affect the site of tetrazolium violet reduction in the electron transport chain of Lactococcus lactis. Microbiol (Read, Engl) 2009;155(Pt 9):2941–8. Epub 2009/06/13. doi: 10.1099/mic.0.029678-0. PubMed PMID: 19520722.
[52] Wu H, Xu P, Huang Y, Wang L, Ye X, Huang X, et al. PCL-1, a trypsin-resistant peptide, exerts potent activity against drug-resistant bacteria. Probiotics Antimicrob Proteins 2021;13(5):1467–80. Epub 2021/05/27. doi: 10.1007/s12602-021-09801-8. PubMed PMID: 34037941.
[53] Xia Y, Cebrián R, Xu C, Jong A, Wu W, Kuipers OP. Elucidating the mechanism by which synthetic helper peptides sensitize Pseudomonas aeruginosa to multiple antibiotics. PLoS Pathog 2021;17(9):e1009909. Epub 2021/09/04. doi: 10.1371/journal.ppat.1009909. PubMed PMID: 34478485; PubMed Central PMCID: PMCPMC8445441.
[54] Baker MR, Zarubica T, Wright HT, Rife JP. Scintillation proximity assay for measurement of RNA methylation. Nucleic Acids Res 2009;37(4):e32. Epub 2009/02/03. doi: 10.1093/nar/gkn1038. PubMed PMID: 19181706; PubMed Central PMCID: PMCPMC2651799.
[55] Husain N, Obranic S, Koscinski L, Seetharaman J, Babic F, Bujnicki JM, et al. Structural basis for the methylation of A1408 in 16S rRNA by a panaminoglycoside resistance methyltransferase NpmA from a clinical isolate and analysis of the NpmA interactions with the 30S ribosomal subunit. Nucleic Acids Res 2011;39(5):1903–18. Epub 2010/11/11. doi: 10.1093/nar/gkq1033. PubMed PMID: 21062819; PubMed Central PMCID: PMCPMC3061052.
[56] Zhao Y, Wang X, Qi R, Yuan H. Recent advances of natural-polymer-based hydrogels for wound antibacterial therapeutics. Polymers 2023;15(15). Epub 2023/08/12. doi: 10.3390/polym15153305. PubMed PMID: 37571202; PubMed Central PMCID: PMCPMC10422483.
[57] Ji JY, Ren DY, Weng YZ. Efficiency of multifunctional antibacterial hydrogels for chronic wound healing in diabetes: a comprehensive review. Int J Nanomed 2022;17:3163–76. Epub 2022/08/02. doi: 10.2147/ijn.S363827. PubMed PMID: 35909814; PubMed Central PMCID: PMCPMC9326039.
[58] Lim CH, Sun Q, Ratti K, Lee SH, Zheng Y, Takeo M, et al. Hedgehog stimulates hair follicle neogenesis by creating inductive dermis during murine skin wound healing. Nat Commun 2018;9(1):4903. Epub 2018/11/23. doi: 10.1038/s41467-018-07142-9. PubMed PMID: 30464171; PubMed Central PMCID: PMCPMC6249328 hair follicle neogenesis and owned by the University of Pennsylvania. M.I. and G.C. have equity in Follica, a start up company that has licensed this patent. All remaining authors declare no competing interests.
[59] Umerska A, Cassisa V, Bastiat G, Matougui N, Nehme H, Manero F, et al. Synergistic interactions between antimicrobial peptides derived from plectasin and lipid nanocapsules containing monolaurin as a cosurfactant against Staphylococcus aureus. Int J Nanomed 2017;12:5687–99. Epub 2017/08/30. doi: 10.2147/ijn.S139625. PubMed PMID: 28848347; PubMed Central PMCID: PMCPMC5557623.
[60] Le CF, Fang CM, Sekaran SD. Intracellular targeting mechanisms by antimicrobial peptides. Antimicrob Agents Chemother 2017;61(4). Epub 2017/02/09. doi: 10.1128/aac.02340-16. PubMed PMID: 28167546; PubMed Central PMCID: PMCPMC5365711.
[61] Cardoso MH, Meneguetti BT, Costa BO, Buccini DF, Oshiro KGN, Preza SLE, et al. Non-lytic antibacterial peptides that translocate through bacterial membranes to act on intracellular targets. Int J Mol Sci 2019;20(19). Epub 2019/10/05. doi: 10.3390/ijms20194877. PubMed PMID: 31581426; PubMed Central PMCID: PMCPMC6801614.
[62] Han HM, Ko S, Cheong MJ, Bang JK, Seo CH, Luchian T, et al. Myxinidin2 and myxinidin3 suppress inflammatory responses through STAT3 and MAPKs to promote wound healing. Oncotarget 2017;8(50):87582–97. Epub 2017/11/21. doi: 10.18632/oncotarget.20908. PubMed PMID: 29152103; PubMed Central PMCID: PMCPMC5675655.
[63] Jantsch J, Schatz V, Friedrich D, Schröder A, Kopp C, Siegert I, et al. Cutaneous Na + storage strengthens the antimicrobial barrier function of the skin and boosts macrophage-driven host defense. Cell Metab 2015;21(3):493–501. Epub 2015/03/05. doi: 10.1016/j.cmet.2015.02.003. PubMed PMID: 25738463; PubMed Central PMCID: PMCPMC4350016.
[64] Berendsen BJ, Elbers IJ, Stolker AA. Determination of the stability of antibiotics in matrix and reference solutions using a straightforward procedure applying mass spectrometric detection. Food Addit Contam Part A, Chem, Anal, Control, Expo Risk Assess 2011;28(12):1657–66. Epub 2011/10/13. doi: 10.1080/19440049.2011.604045. PubMed PMID: 21988199.
[65] Nguyen LT, Chau JK, Perry NA, de Boer L, Zaat SA, Vogel HJ. Serum stabilities of short tryptophan- and arginine-rich antimicrobial peptide analogs. PloS One 2010;5(9). Epub 2010/09/17. doi: 10.1371/journal.pone.0012684. PubMed PMID: 20844765; PubMed Central PMCID: PMCPMC2937036.
[66] Svenson J, Stensen W, Brandsdal BO, Haug BE, Monrad J, Svendsen JS. Antimicrobial peptides with stability toward tryptic degradation. Biochemistry 2008;47(12):3777–88. Epub 2008/03/01. doi: 10.1021/bi7019904. PubMed PMID: 18307313.
[67] Global burden of bacterial antimicrobial resistance in 2019: a systematic analysis. Lancet (London, England). 2022;399(10325):629–655. Epub 2022/01/24. doi: 10.1016/s0140–6736(21)02724–0. PubMed PMID: 35065702; PubMed Central PMCID: PMCPMC8841637.
[68] Yeaman MR, Yount NY. Mechanisms of antimicrobial peptide action and resistance. Pharmacol Rev 2003;55(1):27–55. Epub 2003/03/05. doi: 10.1124/pr.55.1.2. PubMed PMID: 12615953.
[69] Zasloff M. Magainins, a class of antimicrobial peptides from Xenopus skin: isolation, characterization of two active forms, and partial cDNA sequence of a precursor. Proc Natl Acad Sci USA 1987;84(15):5449–53. Epub 1987/08/01. doi: 10.1073/pnas.84.15.5449. PubMed PMID: 3299384; PubMed Central PMCID: PMCPMC298875.
[70] Boman HG, Agerberth B, Boman A. Mechanisms of action on Escherichia coli of cecropin P1 and PR-39, two antibacterial peptides from pig intestine. Infect Immun 1993;61(7):2978–84. Epub 1993/07/01. doi: 10.1128/iai.61.7.2978-2984.1993. PubMed PMID: 8514403; PubMed Central PMCID: PMCPMC280948.
[71] Kalfa VC, Jia HP, Kunkle RA, McCray Jr PB, Tack BF, Brogden KA. Congeners of SMAP29 kill ovine pathogens and induce ultrastructural damage in bacterial cells. Antimicrob Agents Chemother 2001;45(11). 3256-61. Epub 2001/10/16. doi: 10.1128/aac.45.11.3256-3261.2001. PubMed PMID: 11600395; PubMed Central PMCID: PMCPMC90821.
[72] Ebenhan T, Gheysens O, Kruger HG, Zeevaart JR, Sathekge MM. Antimicrobial peptides: their role as infection-selective tracers for molecular imaging. BioMed Res Int 2014;2014:867381. Epub 2014/09/23. doi: 10.1155/2014/867381. PubMed PMID: 25243191; PubMed Central PMCID: PMCPMC4163393.
[73] Zhang L, Rozek A, Hancock RE. Interaction of cationic antimicrobial peptides with model membranes. J Biol Chem 2001;276(38):35714–22. Epub 2001/07/27. doi: 10.1074/jbc.M104925200. PubMed PMID: 11473117.
[74] Ahmad A, Asthana N, Azmi S, Srivastava RM, Pandey BK, Yadav V, et al. Structure-function study of cathelicidin-derived bovine antimicrobial peptide BMAP-28: design of its cell-selective analogs by amino acid substitutions in the heptad repeat sequences. Biochim Et Biophys Acta 2009;1788(11):2411–20. Epub 2009/09/09. doi: 10.1016/j.bbamem.2009.08.021. PubMed PMID: 19735644.
[75] Zhu WL, Song YM, Park Y, Park KH, Yang ST, Kim JI, et al. Substitution of the leucine zipper sequence in melittin with peptoid residues affects self-association, cell selectivity, and mode of action. Biochim Et Biophys Acta 2007;1768(6):1506–17. Epub 2007/04/28. doi: 10.1016/j.bbamem.2007.03.010. PubMed PMID: 17462584.
[76] Pitout JD. Extraintestinal pathogenic Escherichia coli: an update on antimicrobial resistance, laboratory diagnosis and treatment. Expert Rev anti-Infect Ther 2012;10(10):1165–76. Epub 2012/12/04. doi: 10.1586/eri.12.110. PubMed PMID: 23199402.
[77] Kao C, Lin X, Yi G, Zhang Y, Rowe-Magnus DA, Bush K. Cathelicidin Antimicrobial Peptides with Reduced Activation of Toll-Like Receptor Signaling Have Potent Bactericidal Activity against Colistin-Resistant Bacteria. mBio 2016;7(5). Epub 2016/09/22. doi: 10.1128/mBio.01418-16. PubMed PMID: 27651360; PubMed Central PMCID: PMCPMC5030359.
[78] Tredget EE, Shankowsky HA, Rennie R, Burrell RE, Logsetty S. Pseudomonas infections in the thermally injured patient. Burn: J Int Soc Burn Inj 2004;30(1):3–26. Epub 2003/12/25. doi: 10.1016/j.burns.2003.08.007. PubMed PMID: 14693082.
[79] Arampatzioglou A, Papazoglou D, Konstantinidis T, Chrysanthopoulou A, Mitsios A, Angelidou I, et al. Clarithromycin enhances the antibacterial activity and wound healing capacity in type 2 diabetes mellitus by increasing LL-37 load on neutrophil extracellular traps. Front Immunol 2018;9:2064. Epub 2018/09/27. doi: 10.3389/fimmu.2018.02064. PubMed PMID: 30250474; PubMed Central PMCID: PMCPMC6139320.
[80] Feng L, Xu M, Zeng W, Zhang X, Wang S, Yao Z, et al. Evaluation of the antibacterial, antibiofilm, and anti-virulence effects of acetic acid and the related mechanisms on colistin-resistant Pseudomonas aeruginosa. BMC Microbiol 2022;22(1):306. Epub 2022/12/19. doi: 10.1186/s12866-022-02716-6. PubMed PMID: 36529724; PubMed Central PMCID: PMCPMC9762083.
[81] Park J, Oh JH, Kang HK, Choi MC, Seo CH, Park Y. Scorpion-Venom-derived antimicrobial peptide Css54 exerts potent antimicrobial activity by disrupting bacterial membrane of zoonotic bacteria. Antibiot (Basel, Switz) 2020;9(11). Epub 2020/11/26. doi: 10.3390/antibiotics9110831. PubMed PMID: 33233541; PubMed Central PMCID: PMCPMC7699533.
[82] Galera-Laporta L, Comerci CJ, Garcia-Ojalvo J, Süel GM. IonoBiology: the functional dynamics of the intracellular metallome, with lessons from bacteria. Cell Syst 2021;12(6):497–508. Epub 2021/06/18. doi: 10.1016/j.cels.2021.04.011. PubMed PMID: 34139162; PubMed Central PMCID: PMCPMC8570674.
[83] Friedrich T, Steinmüller K, Weiss H. The proton-pumping respiratory complex I of bacteria and mitochondria and its homologue in chloroplasts. FEBS Lett 1995;367(2):107–11. Epub 1995/06/26. doi: 10.1016/0014-5793(95)00548-n. PubMed PMID: 7796904.

[84] Mukherjee A, Ahn YH. Terpinolene as an enhancer for ultrasonic disinfection of multi-drug-resistant bacteria in hospital wastewater. Environ Sci Pollut Res Int 2022;29(23):34500–14. Epub 2022/01/18. doi: 10.1007/s11356-022-18611-6. PubMed PMID: 35037151.
[85] Zhao X, Kuipers OP. BrevicidineB, a new member of the brevicidine family, displays an extended target specificity. Front Microbiol 2021;12:693117. Epub 2021/06/29. doi: 10.3389/fmicb.2021.693117. PubMed PMID: 34177875; PubMed Central PMCID: PMCPMC8219939.
[86] Li Z, Chakraborty P, de Vries RH, Song C, Zhao X, Roelfes G, et al. Characterization of two relacidines belonging to a novel class of circular lipopeptides that act against Gram-negative bacterial pathogens. Environ Microbiol 2020;22(12):5125–36. Epub 2020/07/02. doi: 10.1111/1462-2920.15145. PubMed PMID: 32608161; PubMed Central PMCID: PMCPMC7818431.
[87] Mogi T, Murase Y, Mori M, Shiomi K, Omura S, Paranagama MP, et al. Polymyxin B identified as an inhibitor of alternative NADH dehydrogenase and malate: quinone oxidoreductase from the Gram-positive bacterium Mycobacterium smegmatis. J Biochem 2009;146(4):491–9. Epub 2009/07/01. doi: 10.1093/jb/mvp096. PubMed PMID: 19564154.
[88] Deris ZZ, Akter J, Sivanesan S, Roberts KD, Thompson PE, Nation RL, et al. A secondary mode of action of polymyxins against Gram-negative bacteria involves the inhibition of NADH-quinone oxidoreductase activity. J Antibiot 2014;67(2):147–51. Epub 2013/10/31. doi: 10.1038/ja.2013.111. PubMed PMID: 24169795; PubMed Central PMCID: PMCPMC3943757.
[89] Rowe-Magnus DA, Kao AY, Prieto AC, Pu M, Kao C. Cathelicidin peptides restrict bacterial growth via membrane perturbation and induction of reactive oxygen species. mBio 2019;10(5). Epub 2019/09/12. doi: 10.1128/mBio.02021-19. PubMed PMID: 31506312; PubMed Central PMCID: PMCPMC6737244.
[90] Dwyer DJ, Kohanski MA, Hayete B, Collins JJ. Gyrase inhibitors induce an oxidative damage cellular death pathway in Escherichia coli. Mol Syst Biol 2007;3:91. Epub 2007/03/14. doi: 10.1038/msb4100135. PubMed PMID: 17353933; PubMed Central PMCID: PMCPMC1847949.
[91] Kohanski MA, Dwyer DJ, Hayete B, Lawrence CA, Collins JJ. A common mechanism of cellular death induced by bactericidal antibiotics. Cell 2007;130(5):797–810. Epub 2007/09/07. doi: 10.1016/j.cell.2007.06.049. PubMed PMID: 17803904.
[92] Choi H, Yang Z, Weisshaar JC. Single-cell, real-time detection of oxidative stress induced in Escherichia coli by the antimicrobial peptide CM15. Proc Natl Acad Sci USA 2015;112(3). E303-10. Epub 2015/01/07. doi: 10.1073/pnas.1417703112. PubMed PMID: 25561551; PubMed Central PMCID: PMCPMC4311848.
[93] Hopkin KA, Papazian MA, Steinman HM. Functional differences between manganese and iron superoxide dismutases in Escherichia coli K-12. J Biol Chem 1992;267(34):24253–8. Epub 1992/12/05. PubMed PMID: 1447175.
[94] Lalaouna D, Baude J, Wu Z, Tomasini A, Chicher J, Marzi S, et al. RsaC sRNA modulates the oxidative stress response of Staphylococcus aureus during manganese starvation. Nucleic Acids Res 2019;47(18):9871–87. Epub 2019/09/11. doi: 10.1093/nar/gkz728. PubMed PMID: 31504767; PubMed Central PMCID: PMCPMC6765141.
[95] Sampson TR, Liu X, Schroeder MR, Kraft CS, Burd EM, Weiss DS. Rapid killing of Acinetobacter baumannii by polymyxins is mediated by a hydroxyl radical death pathway. Antimicrob Agents Chemother 2012;56(11):5642–9. Epub 2012/08/22. doi: 10.1128/aac.00756-12. PubMed PMID: 22908157; PubMed Central PMCID: PMCPMC3486575.
[96] Choi H, Yang Z, Weisshaar JC. Oxidative stress induced in E. coli by the human antimicrobial peptide LL-37. PLoS Pathog 2017;13(6):e1006481. Epub 2017/07/01. doi: 10.1371/journal.ppat.1006481. PubMed PMID: 28665988; PubMed Central PMCID: PMCPMC5509375.